

Rayleigh wave phase-velocity heterogeneity and multilayered azimuthal anisotropy of the Superior Craton, Ontario

Fiona A. Darbyshire¹ and Sergei Lebedev²

¹GEOTOP-UQAM-McGill, Université du Québec à Montréal, CP 8888 succursale Centre-Ville, Montréal, QC, H3C 3P8, Canada.

E-mail: darbyshire.fiona_ann@uqam.ca

²Dublin Institute for Advanced Studies, School of Cosmic Physics, Geophysics Section, 5 Merrion Square, Dublin 2, Ireland

Accepted 2008 September 16. Received 2008 August 22; in original form 2008 February 27

SUMMARY

We study the azimuthally anisotropic upper-mantle structure of the Superior Craton and Grenville Province in Ontario, Canada, using Rayleigh wave phase-velocity data in the period range 40–160 s. 152 two-station dispersion measurements are combined in a tomographic inversion that solves simultaneously for isotropic and anisotropic terms using a least-squares technique. We perform a series of tests to derive optimal regularization (smoothing and damping) and to assess the resolution of, and trade-offs between, isotropic and anisotropic anomalies. The tomographic inversion is able to resolve isotropic phase-velocity anomalies on a scale of 200–300 km and to distinguish between different anisotropic regimes on a 500-km scale across the study region.

Isotropic phase-velocity anomalies in the tomographic model span a range of up to ± 2 per cent around a regional average which is similar to the Canadian Shield dispersion curve of Brune & Dorman (1963), with phase velocities up to 3 per cent above global reference models. The amplitude of azimuthal phase-velocity anisotropy reaches a maximum of ~ 1.2 per cent. A clear east–west division of the study area, based on both isotropic phase-velocity anomalies and azimuthal anisotropy, is apparent.

In the western Superior, isotropic phase velocities are generally higher than the regional average. Anisotropy is observed at all periods, with ENE–WSW to NE–SW fast-propagation directions. At periods ≤ 120 s, the anisotropy likely results from frozen lithospheric fabric aligned with tectonic boundaries, whereas the anisotropy at longer periods is interpreted to arise from present-day sublithospheric flow. The fast directions from published *SKS* measurements are close to the fast Rayleigh wave propagation directions throughout the period range sampled, and the large *SKS* splitting times may be accounted for by this near-coincidence of fast-propagation directions. Across most of eastern Ontario, phase velocities are lower than the regional average. Fast-propagation directions rotate from \sim NW–SE at 40–130 s period to WNW–ESE at periods 140–160 s. The results suggest a difference in fast-propagation directions between the anisotropic fabric frozen into the lithosphere and the fabric due to current and recent sublithospheric flow.

The Superior Craton and Grenville Province are characterized by large-scale structural variations that reflect the complex tectonic history of the region. This study highlights differences between the characteristics of eastern and western Ontario and indicates the occurrence of multiple layers of anisotropy in the subcratonic upper mantle.

Key words: Surface waves and free oscillations; Seismic anisotropy; Cratons; Dynamics of lithosphere and mantle.

1 INTRODUCTION

The importance of anisotropy in studies of continental cratons is becoming increasingly apparent as the coverage of teleseismic experiments in these regions increases, and its role in understanding both present-day mantle dynamics and continental tectonic evolu-

tion is widely recognized. Azimuthal anisotropy in the subcontinental lithospheric mantle (particularly the cratonic continental roots) may arise from ‘frozen’ fabric related to past continental deformation and/or alignment of major structural boundaries related to the formation and evolution of the continent (e.g. Silver 1996). Deeper azimuthal anisotropy, beneath the lithosphere–asthenosphere

boundary, may be related to lattice-preferred orientation of mantle olivine formed as a result of present and recent mantle flow.

Surface wave tomography is able to constrain the distribution of azimuthal anisotropy in three dimensions. In particular, variations in surface wave azimuthal anisotropy as a function of period can constrain the depths of anisotropic layers (e.g. Montagner *et al.* 2000), unlike shear wave splitting techniques, which have good lateral resolution but limited depth resolution (e.g. Fouch & Rondenay 2006). Regional-scale studies allow the distribution of seismic anisotropy to be mapped in 3-D on a subcratonic scale, and may provide useful information in understanding the assembly of the continental cratons.

Current regional and continental-scale surface wave tomography methods fall broadly into three categories:

(1) Inversion of surface wave data using relatively short source–station paths. Some techniques are based on the direct inversion of seismic waveforms for shear velocity (e.g. Debayle & Kennett 2000; Simons *et al.* 2002; Friederich 2003; van der Lee & Frederiksen 2005) while others extract phase-velocity information from the data set as a first step in the tomography procedure (e.g. Sebai *et al.* 2006).

(2) Analysis of teleseismic surface waves using closely spaced arrays of broad-band seismographs and assuming ray theory (e.g. Bruneton *et al.* 2002) or a multiple-plane-wave approximation (e.g. Li *et al.* 2003; Weeraratne *et al.* 2003; Forsyth & Li 2005).

(3) Inversions using multiple dispersion curves derived from two-station surface wave analysis across a regional seismic array (e.g. Darbyshire *et al.* 2004; Deschamps *et al.* 2008a).

The issue of model resolution, in particular, the potential trade-offs between isotropic and anisotropic phase-velocity heterogeneities, must be addressed carefully in studies of surface wave tomography that includes a treatment of azimuthal anisotropy. Approaches to the modelling of surface wave anisotropy vary between studies. In some cases (e.g. Debayle & Kennett 2000; Simons *et al.* 2002), 3-D distribution of azimuthal anisotropy is parametrized and inverted for similarly to and together with isotropic shear-speed heterogeneity. Resolution tests are used to assess leakage between isotropic and anisotropic heterogeneities in the models. An alternative approach (e.g. Li *et al.* 2003; Weeraratne *et al.* 2003; Forsyth & Li 2005) is to constrain anisotropy to be uniform across the study region or to vary within defined subregions. In each case, careful assessment of the resolution of the azimuthal anisotropy and the potential for the generation of artificial anisotropy through ‘leakage’ is necessary.

In this paper, we present azimuthally anisotropic Rayleigh wave phase-velocity maps for the Superior Craton. The aim of the study is to constrain lateral variations in fast-propagation direction across the region of interest, and to examine evidence for multiple layers of anisotropy in the region within the depth range spanning the lower crust, subcratonic lithospheric mantle and asthenosphere. An appropriate regularization for the array and for the available data set is derived through a series of tests with different values of smoothing and damping parameters. We also carry out a series of tests to assess the degree of leakage between isotropic and anisotropic phase-velocity heterogeneities, using both the surface wave data and a series of synthetic input models.

The station configuration and surface wave data set discussed in this paper may be regarded as being representative of a typical continental regional seismograph array (with the obvious exceptions of the closely spaced arrays in regions such as Japan and, now, the western USA). The station spacing is in the range 100–300 km, with an irregular geometry, and the azimuthal coverage of interstation

surface wave paths is non-uniform. Path lengths for the surface wave dispersion measurements are in the range 300–1500 km. The assessment of resolution and isotropy/anisotropy trade-off carried out in this study may thus provide useful inferences applicable to the analysis of surface wave data from other continental seismograph arrays.

The anisotropic phase-velocity maps obtained in this study can be used for calculating an azimuthally anisotropic 3-D shear wave velocity model for the region. The 3-D model, along with quantitative joint interpretation of surface wave and *SKS* splitting constraints on anisotropy, will be the focus of a future paper. Here, we concentrate on the derivation and validation of the phase-velocity maps themselves and on the new evidence they provide for multilayered azimuthal anisotropy beneath the region.

2 TECTONIC HISTORY OF THE STUDY REGION

The majority of the study area (Fig. 1) is underlain by the Archean Superior Craton, the largest craton in the world (e.g. Thurston *et al.* 1991). This craton is thought to have been assembled in the ~3–2.6 Ga timeframe, through a progressive accretion of magmatic arc complexes, resulting in a set of tectonic subprovinces with an east–west strike (e.g. Thurston *et al.* 1991; Percival 1996). The Superior Craton is bounded by Proterozoic orogenic belts, including the Trans-Hudson Orogen (~1.8 Ga) to the northwest (NW), the Southern Province (~2.2 Ga) and Penokean Orogen (~1.9–1.6 Ga) to the south and the Grenville Province (~1.1–1.0 Ga) to the southeast (SE) (e.g. Hoffman 1988; Thurston *et al.* 1991; Ludden & Hynes 2000). The southern part of the study area, including Lake Superior and the Nipigon region was affected by the Keweenaw Mid-continent Rift (~1.11–1.09 Ga) event, and the SE of the region contains a graben system and related NW-trending active faults, thought to arise from Laurentian break-up in the late Proterozoic–early Cambrian. Much of the eastern part of the study region has been affected by hotspot volcanism, including the ~2.45 Ga emplacement of the Matachewan dyke swarm (Ernst & Buchan 2001) and the passage of the Great Meteor hotspot beneath North America which resulted in the eruption of kimberlites and volcanics in eastern Ontario (e.g. Heaman & Kjarsgaard 2000).

3 PREVIOUS SEISMIC STUDIES—EVIDENCE FOR ANISOTROPIC STRUCTURE

Darbyshire *et al.* (2007) modelled shear wave velocity structure for a number of representative interstation Rayleigh wave paths across the study region. While this is a well-established method for estimating velocity structure for a regional study, it has limitations due to the averaging of structure along interstation paths that may be several hundred kilometres in length and traverse several tectonic boundaries. The effects of anisotropy are difficult to quantify, and the velocity–depth profiles derived may, therefore, either under- or overestimate the isotropic shear wave speed along a given profile in the presence of an anisotropic mantle.

In the surface wave data set of Darbyshire *et al.* (2007), significant anisotropy in the western Superior is already apparent from an examination of the surface wave phase-velocity curves. All paths traversing the region in an ENE–WSW direction exhibit substantially higher phase velocities than those aligned along different azimuths (Fig. 2). A similar phenomenon was noted by Sol (2003)

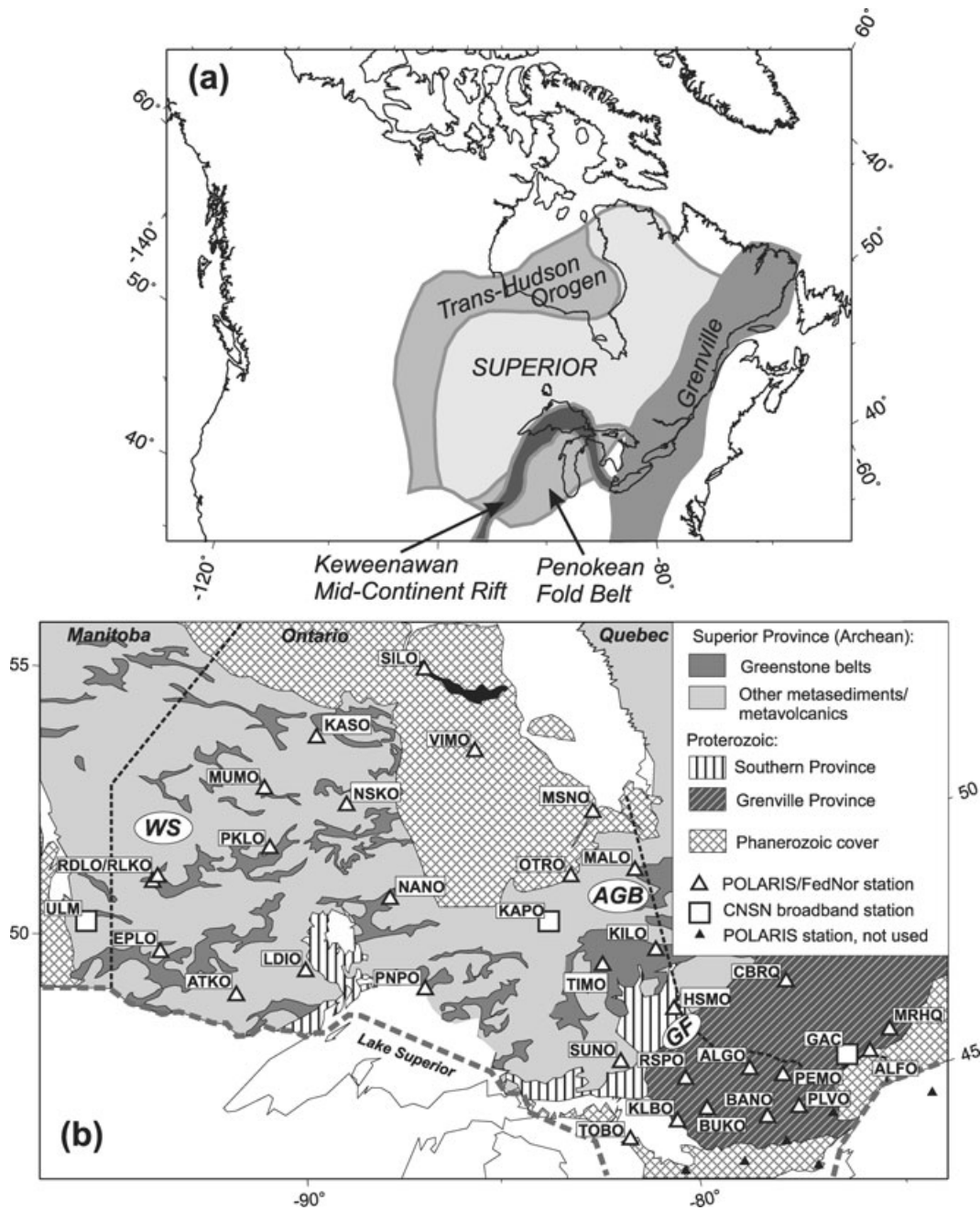


Figure 1. (a) Tectonic map of northern North America, showing the positions of the major tectonic provinces. (b) Map of the study region, showing major geological features and the locations of seismograph stations used in the analysis. Triangles: POLARIS/FedNor stations; squares: permanent broad-band Canadian National Seismograph Network (CNSN) stations. After Darbyshire *et al.* (2007). WS, western Superior; AGB, Abitibi Greenstone Belt; GF, Grenville Front.

when comparing surface wave dispersion curves for N–S and E–W paths across the western Superior. Sol (2003) also inferred the presence of anisotropy from observations of discrepancy between Love and Rayleigh wave dispersion curves and from particle-motion studies of surface waves.

Shear wave splitting studies carried out across the study region over the course of a number of different seismic experiments indicate the presence of significant anisotropy across the region (e.g. Silver & Kaneshima 1993; Kay *et al.* 1999; Rondenay *et al.* 2000a,b; Eaton *et al.* 2004; Frederiksen *et al.* 2006, 2007). SKS splitting times are particularly large—averaging 1.34 s, with a maximum

of 2.1 s (Frederiksen *et al.* 2007)—in the western Superior, and the region is characterized by a consistent ENE–WSW fast direction. In contrast, split times east of $\sim 86^\circ\text{W}$ average 0.67 s, with fast directions scattered around an average E–W alignment. The western Superior fast directions lie subparallel to both the alignment of sub-provincial tectonic belts in the region and to the current absolute plate motion. The anisotropy of the western Superior has largely been interpreted to arise predominantly from frozen lithospheric structural fabric, likely associated with the formation of the Superior Craton by accretion; however Frederiksen *et al.* (2007) point out that anisotropy both due to the alignment of frozen lithospheric

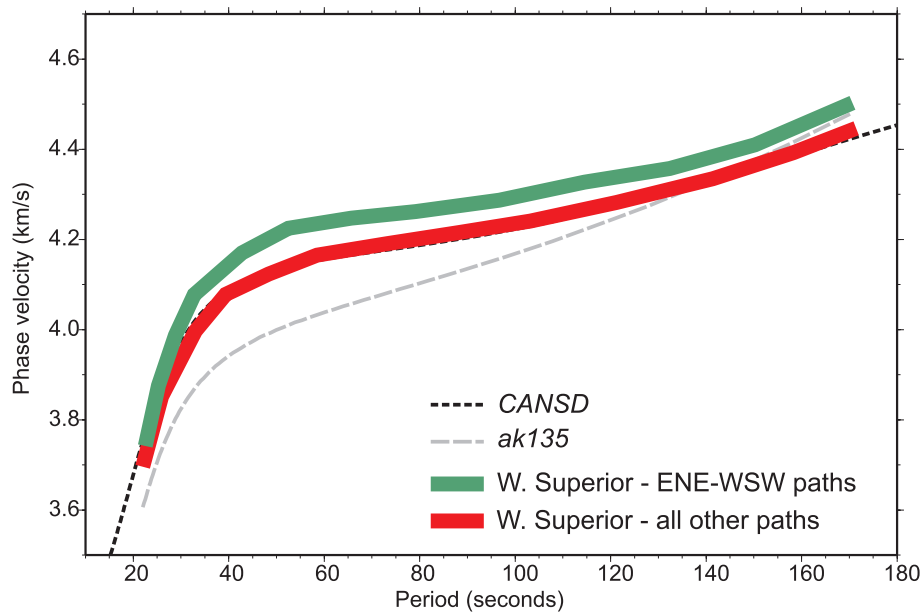


Figure 2. Average dispersion curves from sets of two-station surface wave measurements for paths traversing the western Superior region, showing evidence for anisotropic structure. All paths which cross this region at an ENE–WSW azimuth are characterized by significantly higher phase velocities than those crossing the region at other azimuths.

fabric and due to asthenospheric flow may explain the large split times.

Frederiksen *et al.* (2006) interpreted the *SKS* splitting results for the stations in the east of our study region as arising from a combination of frozen lithospheric fabric and present-day asthenospheric flow. Some variations in splitting characteristics were correlated with known tectonic boundaries, such as the Grenville Front and the subprovince of the Superior Craton immediately to its north. Analysis of receiver function data at Canadian National Seismograph Network (CNSN) station GAC (see Fig. 1) suggested an occurrence of a complex sequence of anisotropic layers in the upper mantle above ~ 120 km depth, with different fast axes, though Frederiksen *et al.* (2006) also noted that a subcrustal anisotropic layer with a NNW–SSE fast direction appeared to be pervasive across the parts of the Grenville Province sampled by receiver function analysis.

The majority of the *SKS* splitting studies carried out in our study region report on the dominant amplitude and direction of splitting, based on an assumption of single-layered anisotropy. One notable exception is the study of Kendall *et al.* (2002), in which results from 45 splitting measurements made at CNSN station ULM (Fig. 1) were examined. The periodicity in the delay times as a function of backazimuth was interpreted to arise from two anisotropic layers. The best-fitting model showed an upper layer aligned with surface geology (fast direction 85°) and existing in the crust and uppermost mantle, whereas the lower layer anisotropy (fast direction 50°) was aligned approximately with absolute plate motion and was interpreted to arise either from fabric frozen into the continental root or a deeper layer of shear flow.

4 DATA SET

We use teleseismic data recorded by a network of temporary broadband seismograph stations deployed in the 2002–2005 time period, primarily across northern and eastern Ontario, as part of the Portable Observatories for Lithospheric Analysis and Research Investigating Seismicity (POLARIS) project (Eaton *et al.* 2005), with addi-

tional support from the Federal Economic Development Initiative for Northern Ontario (FedNor). Data from three CNSN stations are also included in the analysis. The study area is approximately 1200 km east–west and 900 km north–south in extent.

Fundamental-mode Rayleigh wave phase-velocity dispersion curves were estimated for two-station paths across the study region using data from large (typically magnitude 5.5 or higher) teleseismic earthquakes. The two-station method allows path effects between the earthquake source and the seismograph network to be removed, and is, therefore, a popular method in regional studies of lithospheric structure. In total, we were able to obtain dispersion curves for 152 two-station paths (Fig. 3). In general, the phase-velocity data spanned a period range of ~ 30 –180 s, though some curves were more limited in their range. Multiple earthquakes were analysed for each path (typically between 2 and 20 events, with reciprocal source–station paths where possible) to minimize errors due to off-great-circle propagation and multipathing. The description of the data analysis is given in detail by Darbyshire *et al.* (2007) and will not be repeated here.

5 TOMOGRAPHIC INVERSION

The interstation Rayleigh wave dispersion curves are now used as input for a tomographic inversion procedure producing azimuthally anisotropic phase-velocity maps. Each measured interstation dispersion curve $C_i(\omega)$ depends on the structure of the Earth in the area of the two stations. The measurements can be used to constrain the distribution of deviations of phase velocity from a regional average:

$$\int_{\theta} \int_{\phi} K_i(\omega, \theta, \phi) \delta C(\omega, \theta, \phi) d\phi d\theta = \delta C_i(\omega) \pm \Delta C_i(\omega), \quad (1)$$

where θ, ϕ are coordinates, $\delta C(\omega, \theta, \phi)$ is the phase-velocity deviation at a point (θ, ϕ) and frequency ω , $\delta C_i(\omega)$ and $\Delta C_i(\omega)$ are the measured interstation-average phase-velocity anomaly and the measurement error, respectively, and the kernel $K_i(\omega, \theta, \phi)$ defines the sensitivity area for the i th station pair.

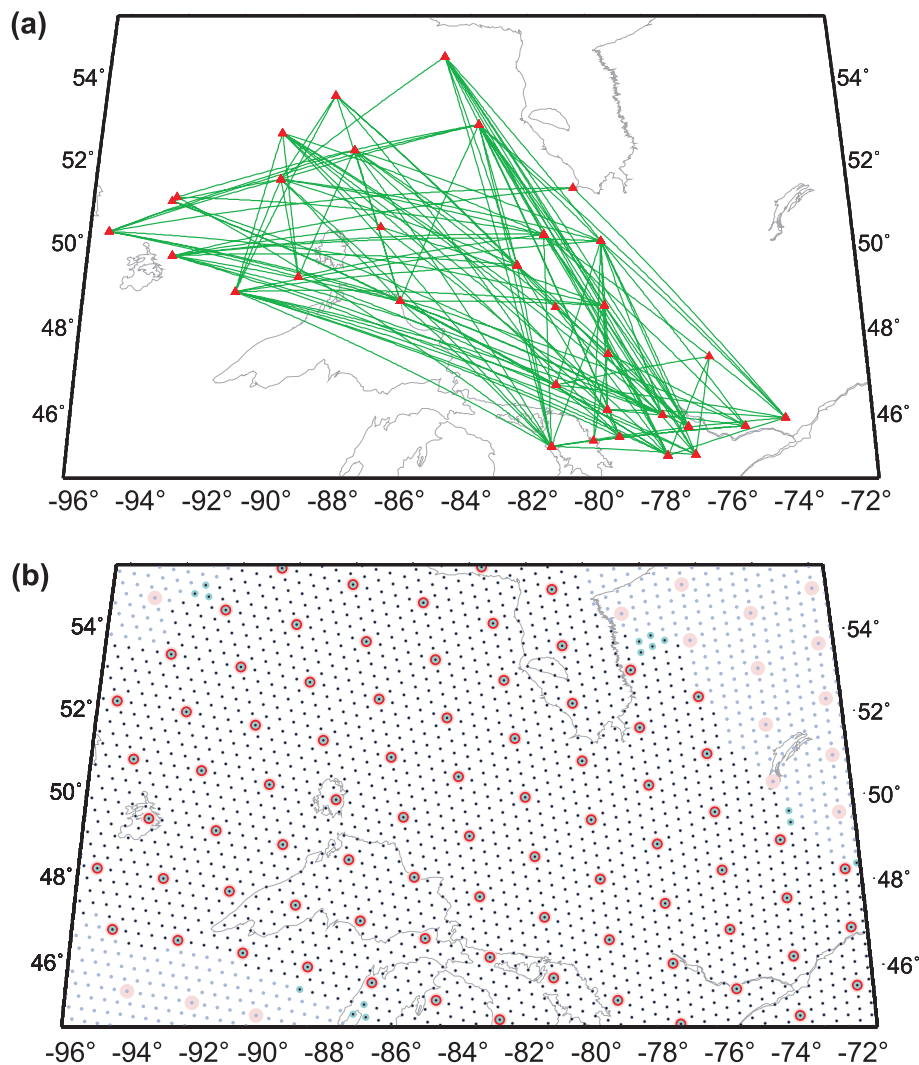


Figure 3. (a) Map of station locations (red triangles) and interstation paths for which surface wave dispersion curves were estimated (green lines), (b) map of integration (green) and model-grid (red) knot points used to parametrize the tomographic inversion.

Differential sensitivity areas corresponding to interstation dispersion measurements are complex, even if estimated with a first-order approximation in a laterally homogeneous Earth (Chevrot & Zhao 2007). The actual small-scale structure of the sensitivity areas will depend on the poorly known small-scale heterogeneity in the Earth through patterns of surface wave diffraction that the heterogeneity gives rise to. Smoothing the sensitivity areas is thus likely to make them more robust.

Prindle & Tanimoto (2006) have tested a number of definitions for smooth differential sensitivity areas in their surface wave study of Southern California and found that the results of phase-velocity mapping depended little on whether geometrical rays or any of the approximate sensitivity areas were used. In this study, we define $K_i(\theta, \phi)$ in the same way at all frequencies ω , normally as zero-width rays along interstation great-circle paths. Finite-width rays were also used in test inversions (Section 6.4). In this case, in the cross-section perpendicular to the path the approximate kernels $K(\theta, \phi)$ are trapezoidal, with a constant kernel value within the middle half of the kernel and a gradual decrease to zero within the peripheral portions.

At 14 selected periods, we combine eq. 1 obtained from all successful dispersion measurements from different station pairs, build

a system of linear equations and solve it using LSQR (Paige & Saunders 1982) with lateral smoothing and (small) norm damping.

Following Lebedev & van der Hilst (2008), the sensitivity areas $K(\theta, \phi)$ are evaluated at knots of a dense integration grid. This global triangular grid of knots with approximately equal interknot spacing is computed as by Wang & Dahlen (1995). The knot spacing for this grid is generally chosen to be a few tens of kilometres (30 km in the case of this study), sufficiently small for an accurate integration over the approximate kernels. For every knot, we identify the hexagon around it that contains all points that are closer to this than any other knot. We compute the areas of these hexagons around the knots (globally, the areas vary by up to 20 per cent). $K(\theta, \phi)$ is calculated at each knot and multiplied by the area of the hexagon around to yield the weight of the knot in the integral over the sensitivity area.

The triangular model grid is constructed like the integration grid but with a larger interknot spacing, chosen according to the station spacing and path coverage in the study region. We choose an interknot spacing of 150 km. Smaller spacing leads to better variance reduction and an increase in small-scale detail in the phase-velocity maps, but likely overfits the data set. Conversely, larger knot spacing leads to an overly smooth map. Phase-velocity perturbations at the

locations of these knots are the unknowns in the inversion. The same shell of knots is used at all periods. The values of $K(\theta, \phi)$ are computed at the model-grid knots by integrating over the neighbouring integration-grid knots. Integration and model-grid knot point locations are shown in Fig. 3.

Our primary smoothing constraints minimize the difference between the anomaly at a knot and the average over anomalies at this and the six (fewer near the boundaries of the region) closest-neighbour knots. This is similar to damping the second derivative of the anomaly distribution. The other type of smoothing constraint we apply is gradient damping, in which the difference between anomalies at every pair of neighbouring knots is penalized (this is similar to damping the first derivative of the anomaly distribution). We use a combination of both types of smoothing, chosen on the basis of visual analysis of resolution test results so as to suppress the leakage between mapped isotropic and anisotropic heterogeneities while not oversmoothing the maps.

Parametrizing isotropic and azimuthally anisotropic heterogeneities, we invert for five unknowns per grid knot:

$$\begin{aligned} \delta C(\omega) = & \delta C_{\text{iso}}(\omega) + A_1(\omega)\cos(2\Psi) + A_2(\omega)\sin(2\Psi) \\ & + A_3(\omega)\cos(4\Psi) + A_4(\omega)\sin(4\Psi), \end{aligned} \quad (2)$$

where $\delta C_{\text{iso}}(\omega)$ is the isotropic phase-velocity anomaly and the ‘ 2Ψ ’ and ‘ 4Ψ ’ terms account for the π - and $\pi/2$ -periodic variations, respectively, of phase velocity with the wave-propagation azimuth Ψ (Smith & Dahlen 1973). Although non-negligible 4Ψ signal has been detected in long-period surface wave studies (Trampert & Woodhouse 2003; Beucler & Montagner 2006), the 4Ψ contribution expected for lattice-preferred alignment of olivine—thought to be the primary cause of anisotropy in the upper mantle—is small (Montagner & Nataf 1986). This may indicate that the mapped 4Ψ anisotropy results, at least in part, from imperfect approximations on wave propagation and structural sensitivity of observables (in particular, the neglect of Love–Rayleigh coupling) rather than from anisotropic properties of the mantle rock. In this study, we allow for 4Ψ heterogeneity but make sure that our main results and conclusions—concerning isotropic and 2Ψ structure—are robust with respect to the amount of the 4Ψ signal allowed in the models.

The strength of smoothing and damping is different for the three different types of unknowns [isotropic: $\delta C_{\text{iso}}(\omega)$; 2Ψ -anisotropic: $A_1(\omega)$ and $A_2(\omega)$; 4Ψ -anisotropic: $A_3(\omega)$ and $A_4(\omega)$]. Because we found that isotropic heterogeneity could be mapped with higher resolution compared to anisotropic heterogeneity, lateral variations in $\delta C_{\text{iso}}(\omega)$ were smoothed less than those in anisotropic terms.

6 NORTHERN ONTARIO PHASE-VELOCITY MAPS—PARAMETERS AND TESTS

The station distribution in this study may be regarded as typical for large regional-scale experiments in continental environments. Station spacing is a few hundred kilometres across most of the study area, with station locations determined by site accessibility and political boundaries. The use of a two-station method in the surface wave analysis also presents restrictions on path coverage due to the standard great-circle requirement inherent in the method. Some interstation paths could not be analysed due to a lack of events near the corresponding great-circle paths. In this section, we explain the choices of optimal smoothing and damping parameters and then focus on the resolution of isotropic and anisotropic phase velocity anomalies. The results of the tests provide some general

inferences on the capabilities of regional-scale passive seismic arrays in imaging anisotropic upper-mantle structure. All tests were carried out using a random-number algorithm to simulate random measurement errors in the phase-velocity dispersion data; the size of the error in each test was chosen to reflect the measurement error appropriate to the relevant period.

6.1 Smoothing and damping

Smoothing and damping are standard means of regularizing a tomographic inversion. Choice of smoothing/damping parameters may be based on examination of trade-offs between model resolution and roughness (e.g. Menke & Abbott 1990). The model roughness is defined as the average difference between the anomaly at a given knot point and the anomalies at its nearest-neighbour grid knots. Oversmoothing results in a lack of resolution that obscures the regional variations of interest, whereas undersmoothing results in good variance reduction but with models dominated by noise due to errors in the data.

Initially, we estimated an appropriate range of smoothing and damping parameters by examining trade-off curves for model roughness against variance reduction for isotropic and anisotropic regularizations. Detailed tests were then carried out to derive the optimal smoothing and damping values for our inversion.

Fig. 4 shows the effects of changes in the strength of the smoothing parameter. The resolution of synthetic isotropic and anisotropic models is tested using the path coverage given by our surface wave data set. As the smoothing increases, the resolution of the features in the synthetic models decreases and is eventually lost. When isotropic anomalies are strongly oversmoothed or overdamped, the signal ‘leaks’ into artificial anisotropic anomalies. A similar, but less-pronounced, effect occurs when anisotropic anomalies are strongly oversmoothed or overdamped.

In the case of an inversion using the data set of surface wave dispersion curves (Fig. 5; 50 s period), the effects of the trade-off between variance reduction and model roughness are also clear. With smoothness constraints too weak, noise due to errors in the dispersion data dominates the resulting phase-velocity maps. The strongest smoothing allows the resolution of only the average velocity and azimuthal anisotropy for the study region as a whole.

Using a series of tests with different regularization settings and different input anomalies, we found, as expected, that isotropic heterogeneity could be constrained with higher resolution compared to anisotropic heterogeneity and thus used lower smoothing and damping parameters for isotropic velocity than for 2Ψ and 4Ψ anisotropies. While the eventual choice of regularization is somewhat subjective, the test series enabled us to explore the potential trade-offs between model parameters and helped us to choose appropriately conservative regularization settings for the inversion of the data set.

6.2 Resolution of isotropic velocity variations—synthetic models

We test the resolution of isotropic velocity variations using a series of synthetic models from which we attempt to recover the structure using the path distribution of the northern Ontario data set at 80 s period; this period gives us the maximum path coverage. Recovery of a gradient in isotropic phase velocity over the study region is good (Fig. 6) with the transition from slow to fast velocities occurring in the correct location. The recovery of the amplitude of the

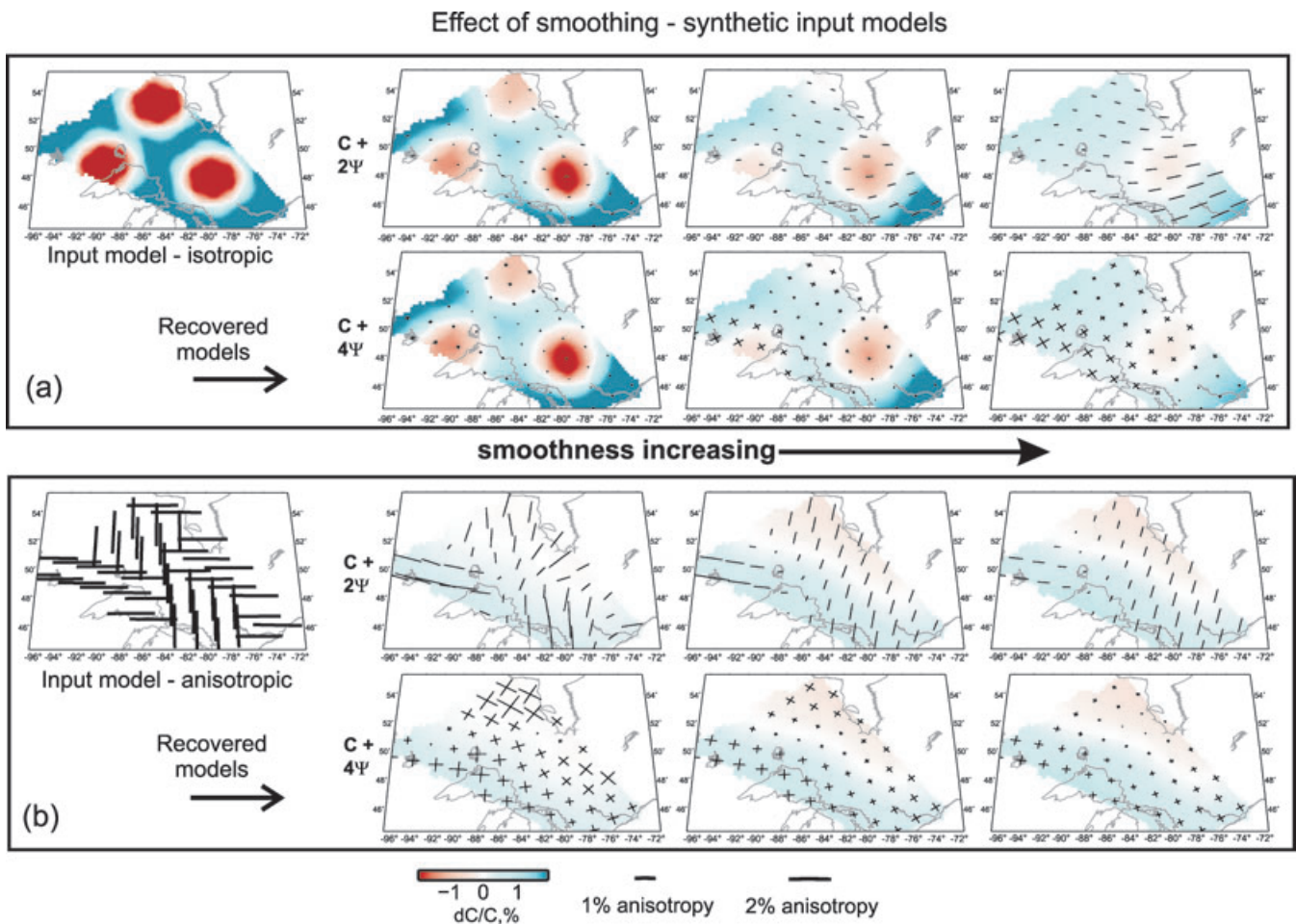


Figure 4. Effect of smoothness constraints on model resolution. (a) Isotropic starting model with low-velocity (red) spike anomalies on a high-velocity (blue) background. The anomaly magnitude is ± 2.4 per cent. (b) Anisotropic synthetic model with a checkerboard pattern of fast directions. Isotropic velocity anomalies are shown in colour; 2Ψ anisotropy is shown as black bars, 4Ψ anisotropy as black crosses.

velocity anomalies is extremely good for the north–south gradient, but amplitude is less well recovered for the northeast (NE)–southwest (SW) gradient, as the highest and lowest velocities in the synthetic model coincide with regions of poorer path coverage. The recovered models show little leakage of the isotropic velocity anomaly into a spurious 2Ψ or 4Ψ signal (see Section 6.3 for details). Due to the regularization of the tomographic inversion (which utilizes damping of the second spatial derivative of each term), we expect the gradient-based resolution tests to give us the best results.

The second resolution test is a spike test (Fig. 7). Pattern *spike3* is composed of a regularly spaced set of knots representing low-velocity anomalies approximately 130 km across; pattern *spike4* results in diamond-shaped low-velocity anomalies 150 km across and 260 km long; pattern *spike5* results in symmetrical low-velocity anomalies 260 km across and pattern *spike6* is similar to a large checkerboard with velocity anomalies ~ 350 km \times 500 km in size. The maximum amplitude of the positive and negative anomalies in the input models is ± 2.4 per cent; the anomaly changes sign abruptly, over a length interval of 150 km at the spike edges.

The recovery of the spike patterns varies depending on both the spatial extent of the anomaly and its position with respect to areas of dense or sparse path coverage. In the case of the ‘spike3’ pattern, the low-velocity anomalies are largely poorly recovered, with the exception of the anomaly located at $\sim 48^\circ\text{N}$, 280°E where

path coverage is particularly dense. Most of the anomalies in the ‘spike4’ pattern show some degree of recovery, though both the amplitude and the spatial extent may vary considerably depending on the position of the anomaly in the original synthetic model. In contrast, the recovery of the ‘spike5’ and ‘spike6’ anomalies is well defined in spatial extent, apart from a small amount of leakage at the model edges, and the recovery of amplitude is significantly improved compared to the smaller anomalies.

The tests indicate that the path coverage in the study area and the parametrization of the inversion is sufficient to provide an adequate recovery of phase-velocity anomalies of 200–300 km in width across the majority of the study area. Anomalies of 100–200 km in width may be recovered in the regions that have the densest path coverage.

6.3 Is anisotropy necessary?

The tomographic inversion is set up in a way that allows us to invert the dispersion data set solely for isotropic phase-velocity anomalies or for the full anisotropic solution. By assessing the differences between the resulting models, we can argue that the inclusion of anisotropy in the inversion significantly improves the solution. When an isotropic solution is forced, the resulting phase-velocity maps are qualitatively similar to those provided in

Effect of smoothing - dispersion data at 50 seconds period

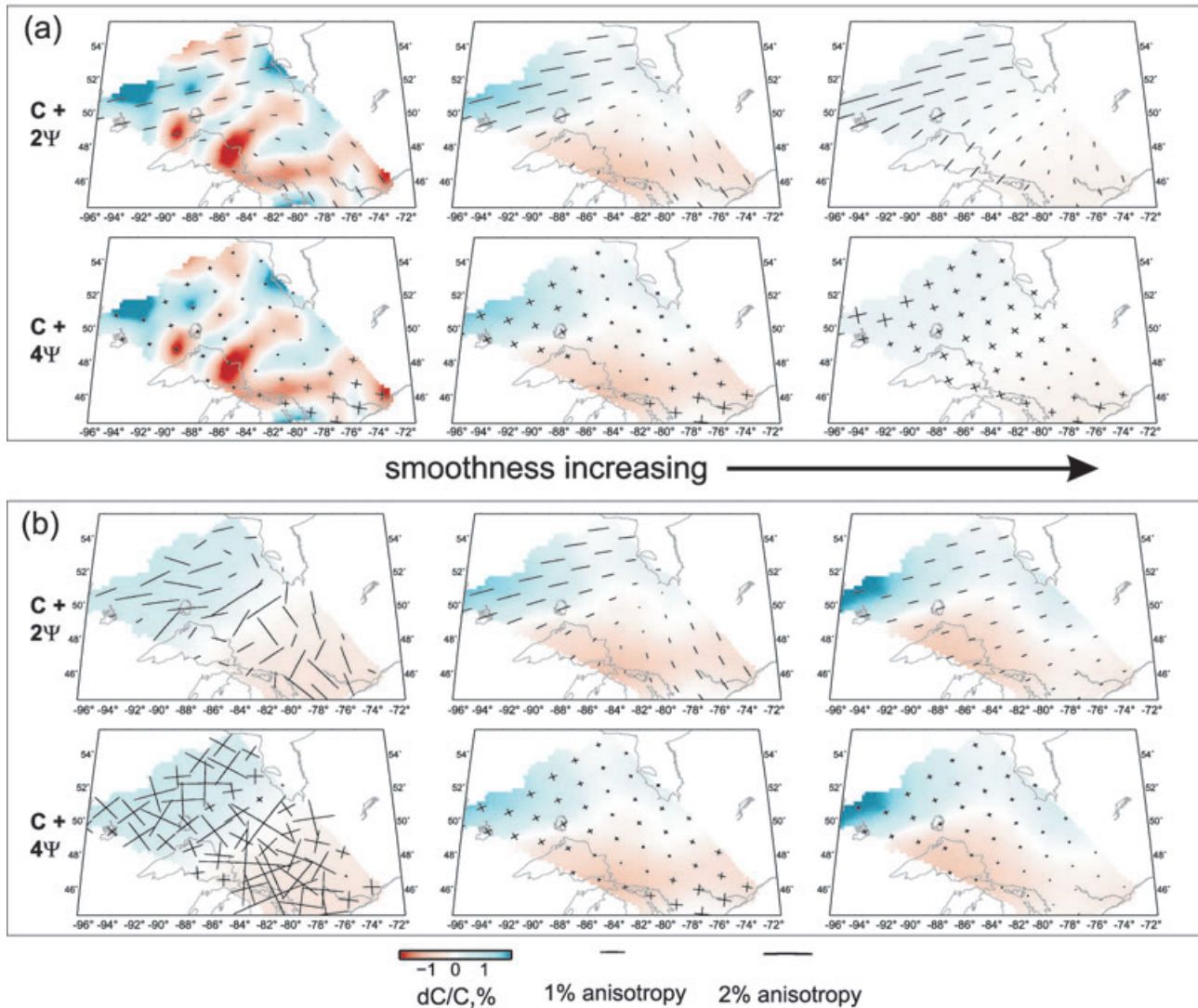


Figure 5. Phase-velocity map for dispersion data at 50 s period, showing the effects of increasing smoothing of (a) isotropic phase velocity (with 2Ψ and 4Ψ smoothing parameters kept constant) and (b) anisotropy (2Ψ and 4Ψ , with isotropic smoothing parameters kept constant). Plotting conventions as for Fig. 4.

the full solution, but the maximum amplitudes are larger by a factor of 2. The strongest effect is observed in the west of the study region, where evidence for strong anisotropy is provided by previous geophysical studies. Inclusion of anisotropy in the inversions typically improves the variance reduction by ~ 25 per cent. The results suggest that interpretation of an isotropic phase-velocity map would not lead to errors in the assessment of structural variation across the study area, but that velocity heterogeneity would be overestimated if anisotropy was neglected.

6.4 Leakage between isotropic and anisotropic structures

An important consideration in a tomographic inversion that solves for both isotropic and anisotropic parameters is the question of artefacts arising from leakage between isotropic velocity heterogeneities and azimuthal anisotropy. We used tests based on both synthetic models and on real data sets to examine the extent of leakage in the study area.

6.4.1 Leakage in a real data set

We first tested for leakage by taking a phase-velocity map calculated from the Rayleigh wave data set at a given period, removing either the isotropic or anisotropic part, and reinverting it to assess the recovery of the desired parameter and leakage into the removed parameters (Fig. 8). We carried out the test at periods of 60, 120 and 160 s and found that, in general, the leakage between isotropic phase velocity and 2Ψ and 4Ψ anisotropies was small. A 1.6–1.8 per cent peak-to-peak isotropic wave speed variation across the entire study region generated an average of 0.06–0.1 per cent artificial anisotropy (compared to 0.9 per cent anisotropy in the full phase-velocity maps). The exception was a higher amount (0.2–0.6 per cent) of spurious anisotropy at the edges of the models, where the azimuthal path coverage is poor. In these peripheral areas, the retrieved anisotropy is not robust and is not plotted when discussing the results of the inversion of the data (Section 7).

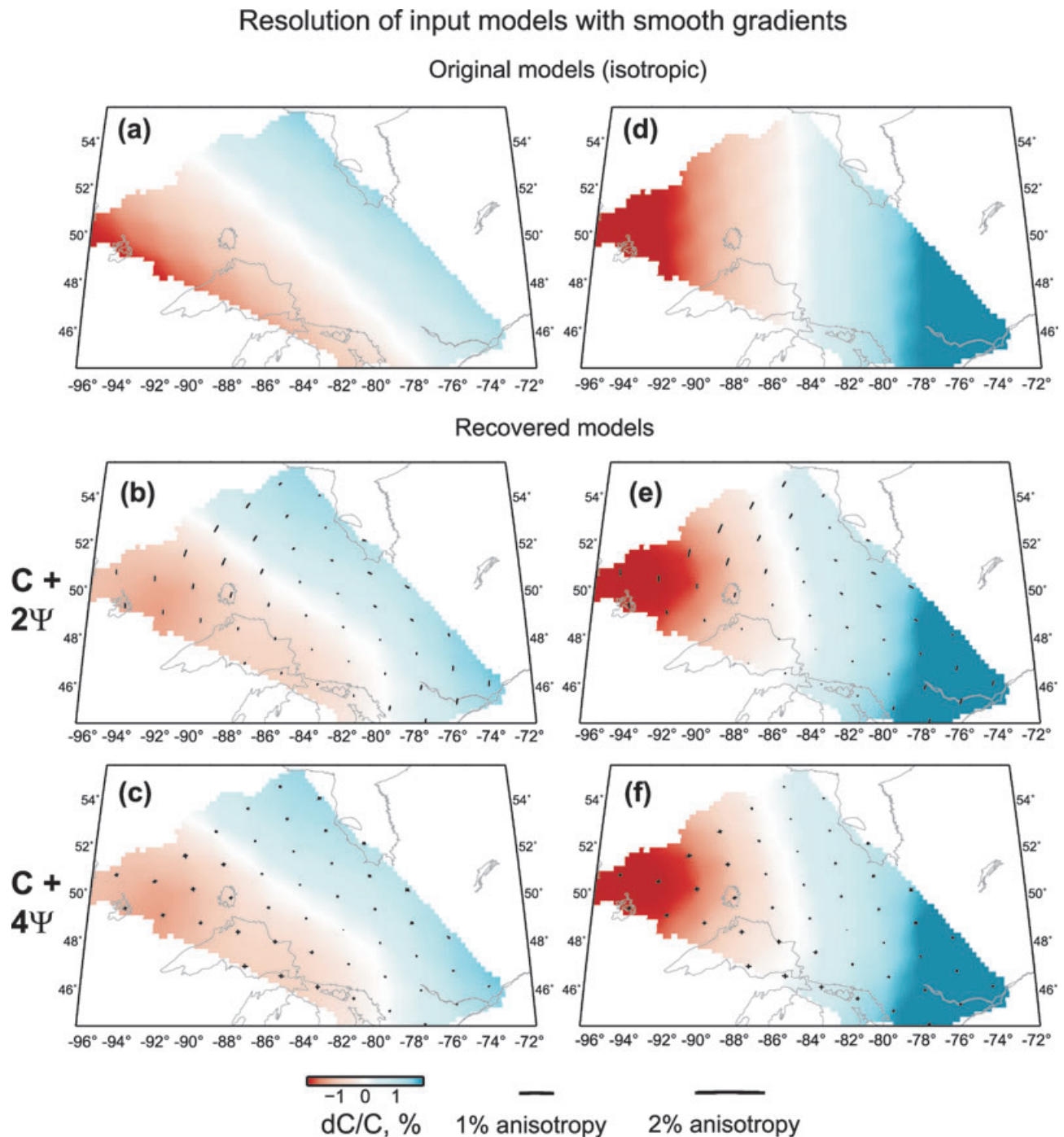


Figure 6. Resolution of isotropic synthetic models for which the phase-velocity anomaly changes as a gradient. (a) and (d) Original synthetic models; (b) and (e) isotropic anomaly and 2Ψ anisotropy; (c) and (f) isotropic anomaly and 4Ψ anisotropy.

6.4.2 Leakage from synthetic isotropic starting models

The results of resolution tests based on gradients of velocity across the model space show very little leakage between isotropic and anisotropic anomalies. For an input range of 3–6 per cent isotropic velocity anisotropy distributed evenly across the model space, an average of 0.1 per cent spurious anisotropy was created in the models when they were inverted.

The spike tests produced a more significant amount of spurious signal in both 2Ψ and 4Ψ anisotropies (Fig. 7). Inspection of

the patterns of the spurious anisotropy shows considerable variation in both amplitude and fast direction depending on the spatial extent and position of the original isotropic velocity anomalies. The artificial anisotropy shown in the spike tests can be attributed to the high degree of isotropic heterogeneity in the input models; in particular, their large variation in isotropic phase-velocity anomaly (almost 5 per cent) over a short spatial distance (~ 150 km). In this case, the amount of artificial anisotropy produced (0.3–0.4 per cent) is comparable to the observed anisotropy in our real data. The strong, small-scale isotropic heterogeneity that gives rise

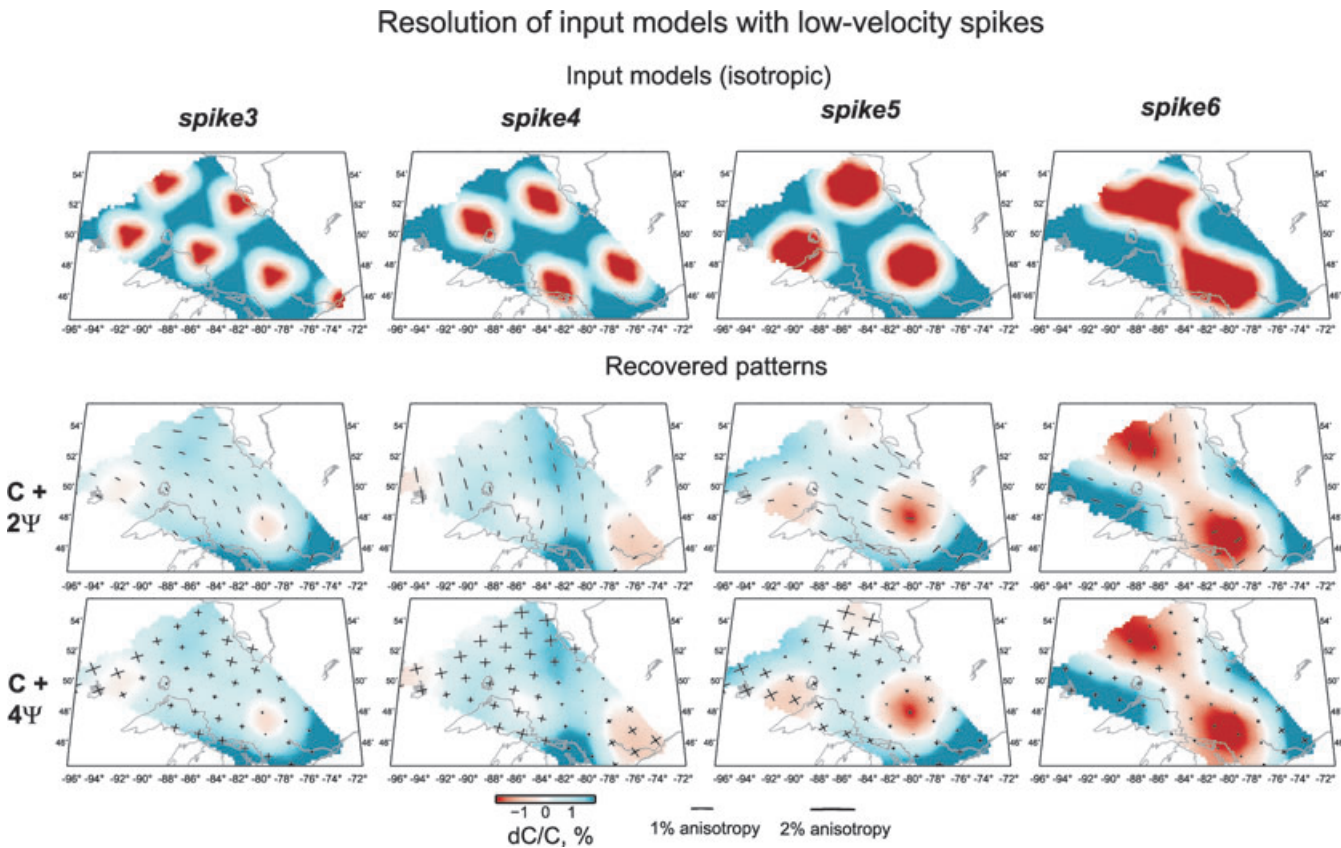


Figure 7. Resolution tests for isotropic low-velocity spike anomalies of varying sizes. In each case, the anomaly magnitude is ± 2.4 per cent.

to these trade-offs, however, is also recovered in the isotropic output of resolution tests (Fig. 7), albeit with a reduced amplitude. An exception is the smallest-scale anomalies (*spike3*) in the parts of the region with sparse sampling. It follows that if sufficiently strong small-scale heterogeneity was present in the region to cause leakage artefacts that could dominate the anisotropy we have mapped, then we would also be likely to see an expression of this heterogeneity in our isotropic models. We do not see this in our observations, which suggests that the effect of the trade-offs on the smooth distributions of anisotropy that we have imaged is likely to be limited.

6.4.3 Recovery of anisotropy fast directions

To further investigate the degree of leakage in the models, we took the phase-velocity maps derived from the surface wave data set, rotated the 2Ψ anisotropy bars through 90° , set the 4Ψ anisotropy values to zero and reinverted the resulting synthetic model (*cf.* Zhang *et al.* 2007). A significant shift in fast direction of the final recovered model would indicate that the original data set had unacceptable leakage between isotropic and anisotropic anomalies, or spurious anisotropy arising from path bias. The results of the test are shown in Fig. 9. The periods used in the test are those with the most heterogeneous distribution of fast directions; artificial anisotropic anomalies resulting from leakage or path coverage effects would be expected to be strongest for these periods, if such artefacts affect the inversion. The results of the test indicate a good recovery of the fast directions of the rotated 2Ψ anisotropy bars and minimal leakage into 4Ψ anisotropy—spurious 4Ψ values average ~ 0.07 per cent, compared to 2Ψ values averaging 0.22 per cent

across the model space. This test supports our assertion that the mapped anisotropy fast directions are robust.

6.4.4 Leakage tests—conclusion

The spike tests demonstrate the potential for significant isotropy/anisotropy trade-offs when the model is highly heterogeneous. Careful assessment of the surface wave tomography results is required for every data set and every study region. In this study, our series of test inversions of synthetic and real data suggest that the smooth patterns of anisotropy that we have mapped are robust, with the impact of the trade-offs on them sufficiently small to allow confidence in our interpretations.

6.5 Path coverage and path width

The path coverage of the data set is non-uniform across the region of study, due primarily to the distribution of suitable teleseismic events, constrained by the requirement for near-great-circle propagation in two-station dispersion analysis and to the restrictions on the locations of stations in the array. We tested the effects of removing or averaging subparallel paths to provide more uniform path coverage, and found that the effect on the resolved phase-velocity patterns was minimal.

The tomographic method described here uses the traditional ray representation of the interstation surface wave sensitivity; however, it is also possible to assign a finite path width to each interstation path, to approximate a broad sensitivity area (kernel) in the inversion (Section 5). For finite path widths extending to several hundred kilometres around the interstation ray path, the tomographic

Leakage tests for phase velocity map at 60 seconds period

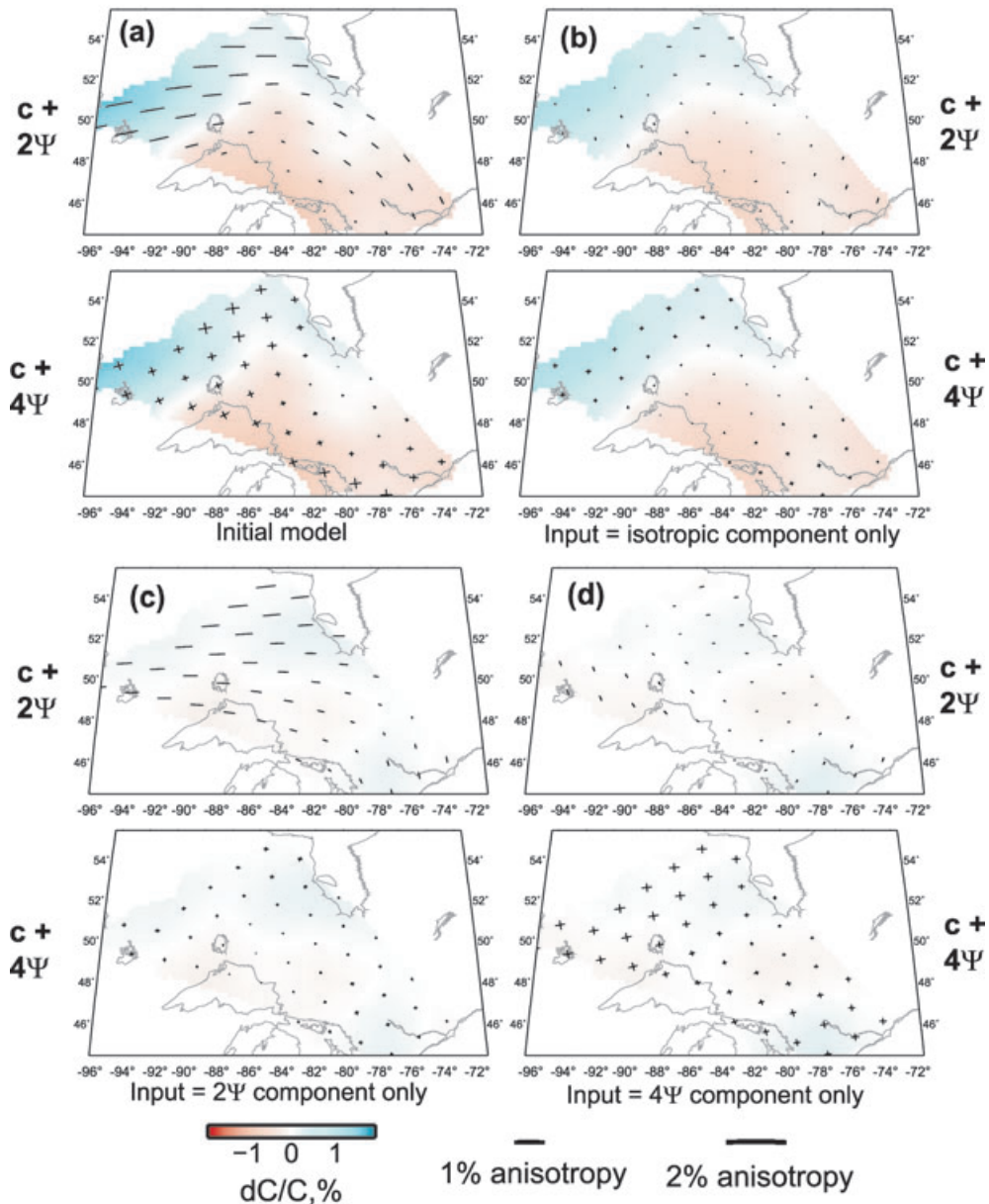


Figure 8. Leakage tests based on phase-velocity map from surface wave data at 60 s period. (a) Original phase-velocity map; starting model using (b) isotropic component only, (c) 2Ψ component only, (d) 4Ψ component only.

inversion produces phase-velocity maps that are almost identical to those calculated using zero-width rays. At 1000 km path width, comparable to the north–south extent of the entire study area, the phase-velocity maps remain qualitatively similar. Inspection of the values of maximum and average anisotropic anomalies indicates no systematic change in the results as a consequence of finite path width, except for a slight decrease in variance reduction as the path width increases.

7 NORTHERN ONTARIO PHASE-VELOCITY MAPS

The average isotropic phase velocity for the study region as a whole is calculated at each period, and the results are shown in Fig. 10.

The dispersion curve lies extremely close to the average Canadian Shield curve ‘CANSD’ of Brune & Dorman (1963), which is derived from a compilation of measurements of interstation phase velocity across Canada, with the exception of the western Cordillera. Paths used in the study cross much of the Canadian Shield, including a combination of largely cratonic paths and paths sampling both cratons and Proterozoic mobile belts. The Canadian Shield average dispersion curve lies above those derived from global reference models such as AK135 (Kennett *et al.* 1995; shown in Fig. 10) up to ~ 140 s period. The maximum phase-velocity anomaly lies in the 40–80 s period range and has an amplitude of ~ 3 per cent.

Fig. 11 shows anisotropic maps of the distribution of phase velocities at periods from 40 to 160 s, sensitive to seismic structure

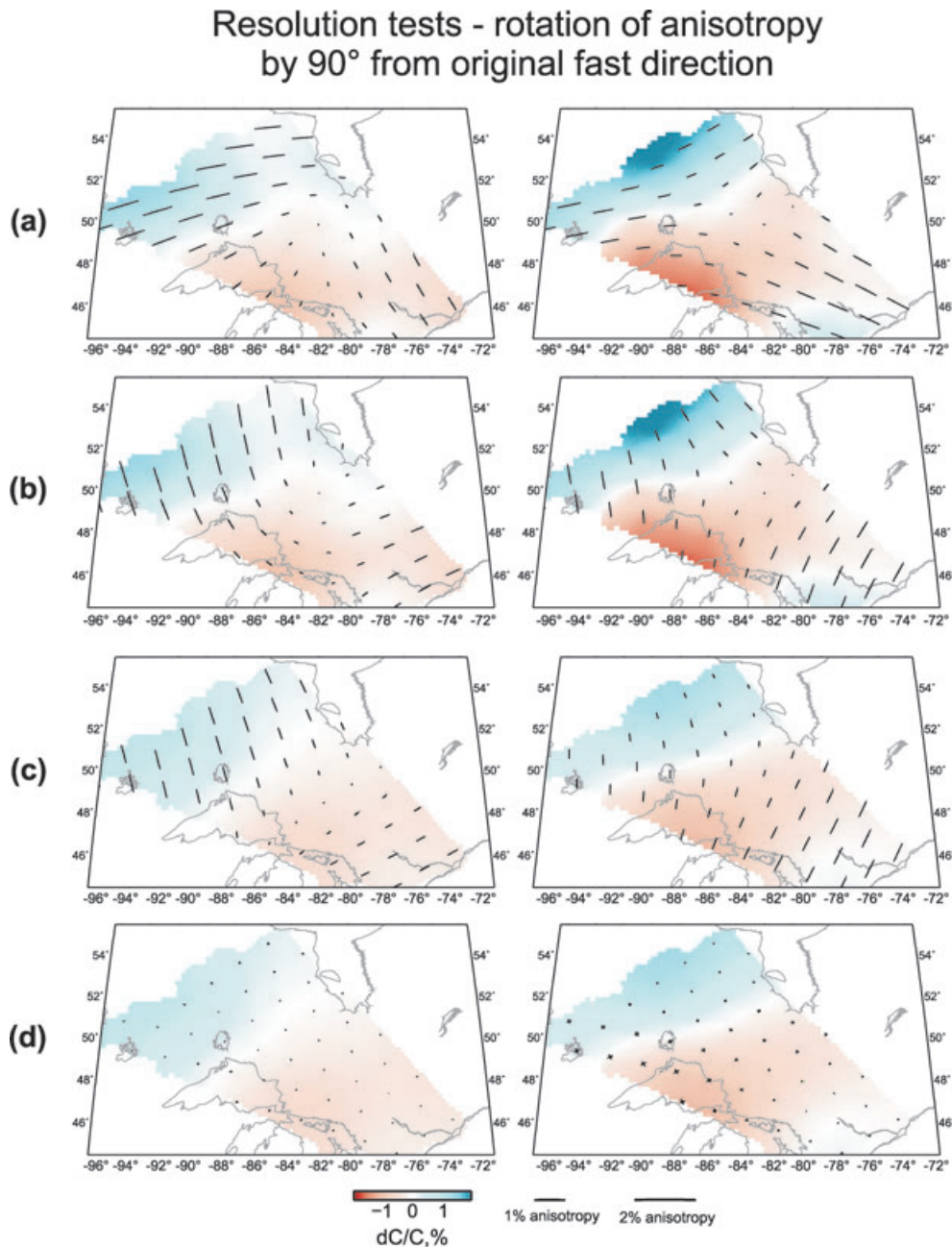


Figure 9. Results of anisotropy leakage test in which the starting model is taken from the original phase-velocity map, but with 2Ψ anisotropy directions rotated by 90° and 4Ψ anisotropy set to zero. (a) Original phase-velocity map, (b) map with rotated anisotropy used as input, (c) and (d) results of inversion for isotropic phase velocity plus 2Ψ and 4Ψ anisotropy values, respectively.

in a depth range from the lower crust/uppermost mantle to the asthenospheric upper mantle. Isotropic phase velocities are shown with colours shaded from red (slower than average for the given period) to blue (faster than average for the given period) and show a range of up to ± 2 per cent around the average for the region. The patterns of isotropic velocity perturbation vary with period but, for periods of 50–160 s (at which Rayleigh waves sample primarily the mantle lithosphere and uppermost asthenosphere), certain features are consistent. The highest phase velocities are associated with the northern and western regions, though the largest anomaly shifts position from the western Superior to the northcentral Superior for periods of 120 s or more. The Great Lakes, the central region of the study area and the Superior Craton in the east of the study

region are characterized by lower than regional-average phase velocities, with a particularly strong low-velocity anomaly appearing beneath central and eastern Lake Superior at long periods. At periods greater than 80 s, higher than average phase velocities appear in the southeastern section of the study region, corresponding to the Proterozoic Grenville Province. The high phase velocity is particularly pronounced in the period range 100–130 s (corresponding to the lower lithosphere), but appears to shrink and to shift position south and west at longer periods.

The fast phase velocities associated with the region as a whole are particularly apparent when the maps are plotted against phase velocities derived from the AK135 global reference model (Kennett *et al.* 1995). Phase velocity is consistently higher than AK135 across

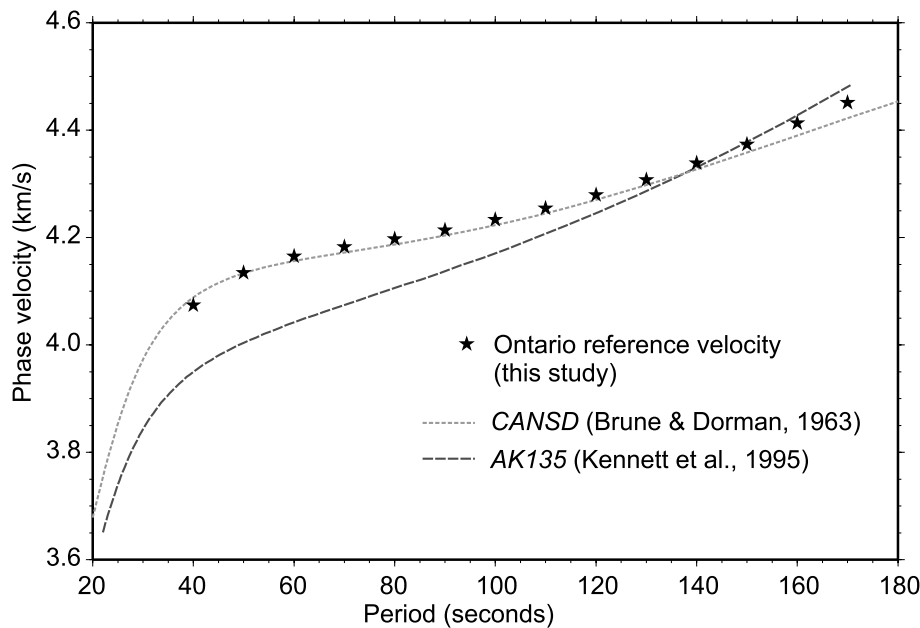


Figure 10. Dispersion curves showing the average dispersion for the region (stars) compared to the CANSD Canadian Shield reference (Brune & Dorman 1963) and a dispersion curve derived from the global reference AK135 (Kennett *et al.* 1995).

the entire study region up to periods of ~ 100 s. At longer periods, velocities below those of the AK135 model appear first beneath the Lake Superior region, then spread throughout central and eastern Ontario. The northwestern Superior remains faster than the global reference throughout the period range sampled by the surface waves.

Patterns of azimuthal anisotropy also vary with period. To examine these variations more closely, we distinguish three regions in our interpretation: western (areas west of 87° W), central (approximately 82° W– 87° W) and eastern ($<82^\circ$ W). It is clear from the tests shown in the previous section that the resolution of the tomographic inversion is sufficient to constrain regional variations in anisotropy patterns at this scale.

(1) Western region: This region is characterized by relatively strong anisotropy, trending in an E–W to NE–SW direction. Between 40 and 90 s period, the dominant direction is ENE–WSW, and the amplitude of anisotropy gradually decreases with increasing period from its maximum at 40 s (sampling primarily the lower crust and uppermost mantle). At 100–110 s, anisotropy is weak and no dominant fast direction is apparent. However, for periods of 120 s and more, a pattern of NE–SW to ENE–WSW anisotropy is again established, with the areas of highest amplitude corresponding to the regions of anomalously high isotropic velocity.

(2) Central region: Azimuthal anisotropy is at its weakest in the central region of the study area, particularly in the period ranges 60–100 and 120–150 s. It is not apparent that a coherent anisotropy pattern occurs over the extent of this region, and it is possible that it may simply represent a zone of transition between the anisotropic regimes in the east and west.

(3) Eastern region: For periods up to 140 s, the eastern region is characterized by NW–SE-trending anisotropy. The signals are weak in comparison with those of the western region for periods <100 s but the magnitude of the anisotropy increases at longer periods. At the longest periods (160 and 170 s), fast-propagation directions rotate towards a WNW–ESE direction.

7.1 Comparison of anisotropy directions with results from SKS splitting studies

Fig. 12 shows a compilation of SKS splitting results for the region (Frederiksen *et al.* 2007), together with the directions of absolute plate motion from Nuvel1-NNR (Argus & Gordon 1991) and the fast anisotropy directions from this study that are considered to be well resolved. Two cases are given; the results from the preferred smoothing parameters and the results from the case where the anisotropic components of smoothing and gradient damping are substantially increased (yielding regional-average anisotropy patterns). The amplitudes of the surface wave and SKS splitting results are not scaled; here we compare only the fast-propagation anisotropic directions.

In both cases, we note a close match between SKS and surface wave fast directions throughout the western half of the study region (west of 85°), for all periods sampled. These results suggest that the western SKS splits are influenced by anisotropic fabric throughout the entire depth range sampled by the surface wave study, within which there is little change in fast direction. The results suggest that the coincident fast directions over the entire depth range reinforce one another and contribute to the large (average 1.34 s) SKS splits observed in the west.

Kendall *et al.* (2002) interpreted backazimuthal variations in SKS splitting properties at station ULM as arising from two anisotropic layers with fast directions of 85° and 50° . Station ULM is situated at the far western corner of the array, preventing detailed comparisons between SKS and surface wave results *in situ*. However, it is of note that the surface wave results for the western Superior show similar variations in average fast direction, from 75° – 90° at periods of 40–90 s to 50° – 60° in the 110–130 s period range, and rotating back to a 70° – 85° range for periods of 140 s and more.

East of $\sim 85^\circ$ W, the relation between fast-propagation directions inferred from SKS splitting and from our surface wave tomography is not as clear. Taking first the case of the results from a heavily smoothed tomographic inversion, we note that the \sim E–W fast direction agrees fairly well with the average SKS splitting direction and with the direction of absolute plate motion. In contrast, the

Results - phase velocity maps relative to regional average at each period

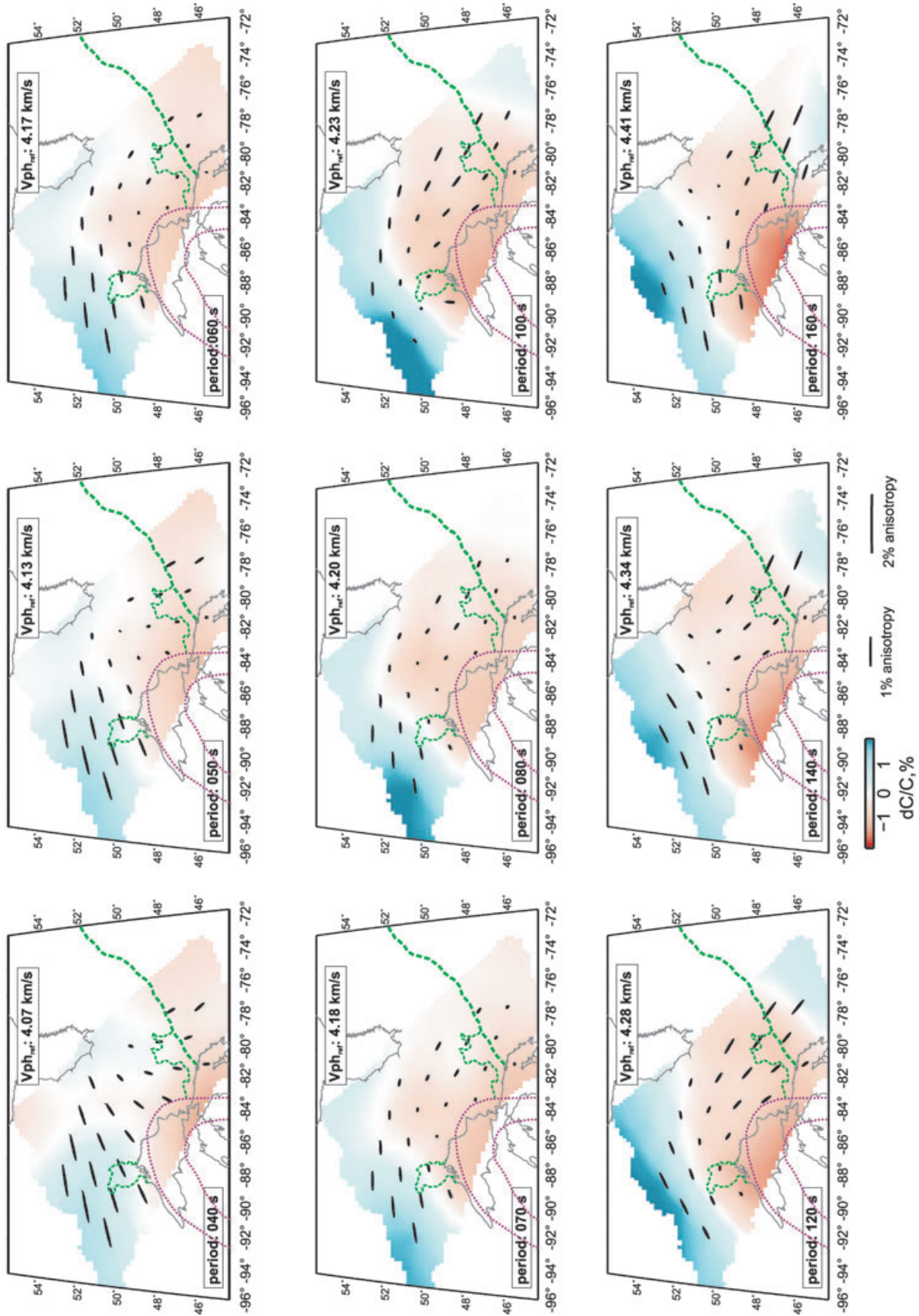


Figure 11. Results: anisotropic phase-velocity maps for the study region, showing isotropic phase-velocity anomaly and 2% anisotropy. In each case, the isotropic phase-velocity is plotted relative to the average phase velocity for the given period (labelled on each panel). Anisotropy results are shown only where azimuthal path coverage is sufficient for the results to be robust. Green dashed lines (see Fig. 1 for details); purple dashed lines—approximate location of the Keweenaw Mid-continent Rift.

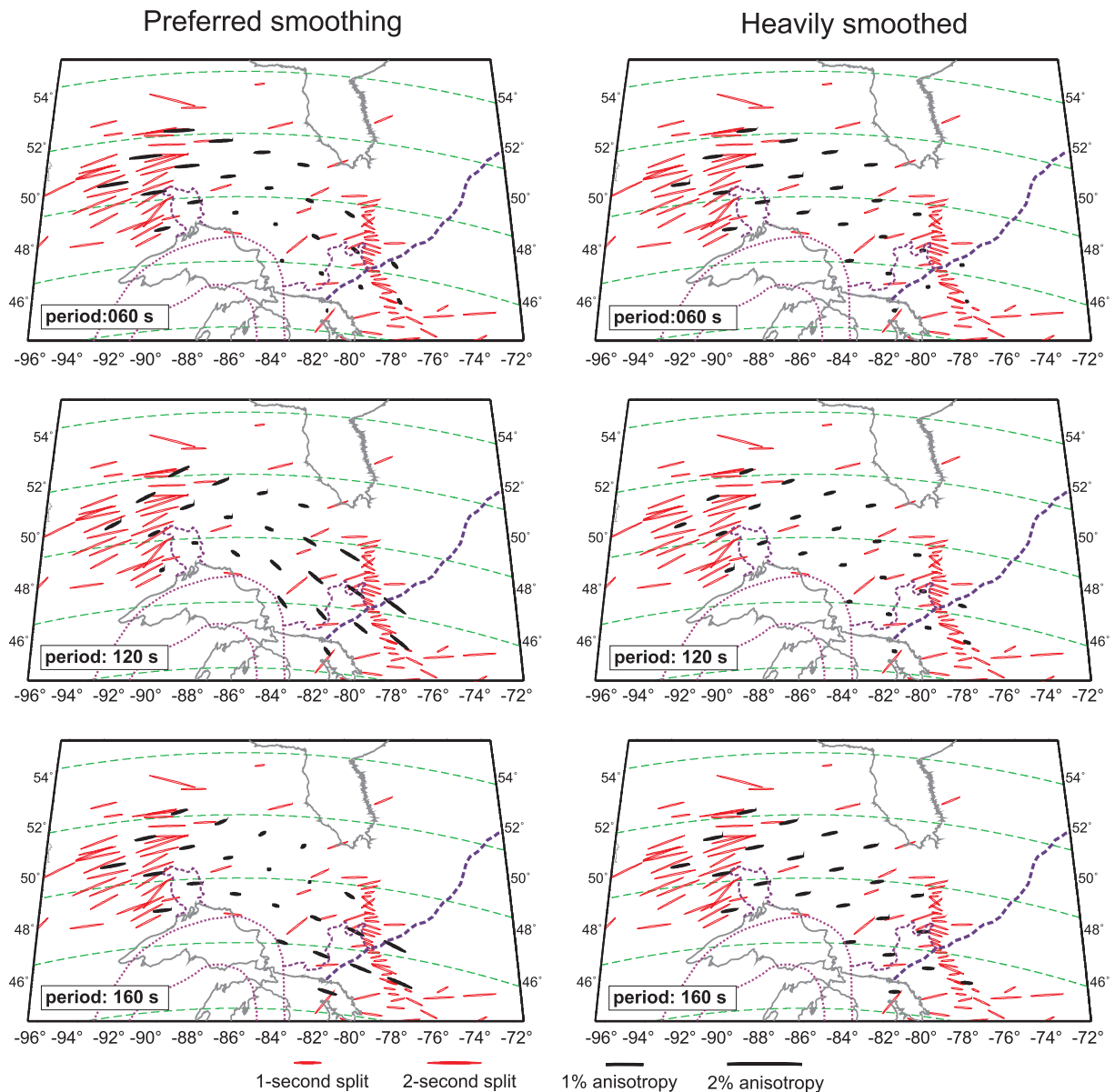


Figure 12. Comparison of anisotropic fast directions from *SKS* splitting measurements (red bars; Frederiksen *et al.* 2007) and surface wave phase velocities at 60, 120 and 160 s (black bars; this study). Green dashed lines—absolute plate motion (Argus & Gordon 1991). Left-side panels: anisotropy calculated using our preferred smoothing parameters as inferred from resolution tests, right-side panels: heavily smoothed solution for surface wave anisotropy. Purple dashed lines—tectonic boundaries.

results from the less-smoothed inversion show a NW–SE fast direction in the east of the study region at most periods, rotating to a more WNW–ESE direction at the longest periods studied (140–160 s), at which Rayleigh waves sample both the lower lithosphere and the asthenosphere. *SKS* splitting results in the $\sim 80^{\circ}\text{W}$ – 85°W region show an E–W to ENE–WSW average fast direction. However, the variability in fast direction exhibited by the ABI-96 stations (Rondenay *et al.* 2000a,b; shown as a dense N–S line of splitting measurements) is such that several of the splits line up with the NW–SE fast directions inferred from the surface wave tomography. The WNW–ESE fast direction of many of the splitting directions, along with the surface wave results at the longest periods, also lies subparallel to the direction of absolute plate motion in this region.

8 DISCUSSION

The use of a tomographic method that separates out the effects of isotropic velocity heterogeneity and azimuthal anisotropy is extremely valuable in the study of continental cratons, many of which have been shown to exhibit significant anisotropy (e.g. Debayle & Kennett 2000; Sebai *et al.* 2006). The isotropic phase-velocity maps can constrain the physical structure of the lithosphere and asthenosphere. Anisotropy provides information on the history of deformation in the subcratonic crust and mantle. The period-dependence of the surface wave signals allows us to place constraints on the depth extent and the origin of the anisotropic signal.

Subcontinental-scale studies often utilize arrays of seismograph stations with a typical station spacing of a few hundred

kilometres, and two-station phase-velocity analysis using large teleseismic earthquakes is generally well suited to this type of array configuration. Great-circle-path considerations and uneven distribution of seismograph stations may lead to non-uniform path coverage over the region of study. In this situation, it is important to gain qualitative and quantitative information about the scale of the structures that can be resolved, and the degree to which data error or path bias may affect the results of the study.

With the data set used in this study, isotropic phase-velocity anomalies of ~ 200 – 250 km in width may be resolved throughout the study area and, in the regions of densest path coverage, it is possible to resolve anomalies as small as ~ 150 km in width. The tests presented in this paper suggest that it is possible to resolve differences in anisotropic fabric over length scales of ~ 500 km. Vertical resolution is controlled by the sensitivity kernels of the Rayleigh waves. We are able to detect layering in anisotropy within the depth range sampled by the data set, representing a considerable improvement over the vertical resolution afforded by *SKS* splitting measurements. The resolution of isotropic and anisotropic anomalies beneath the study region allows us to model the structure of the Superior Craton on a subprovincial scale, and to investigate the correlations between surface tectonic boundaries and mantle velocity anomalies.

Isotropic phase velocity is higher in the western Superior than the central and eastern Superior within our study region, broadly consistent with the findings of Frederiksen *et al.* (2007), using body wave tomography. The lowest phase velocities occur beneath Lake Superior, particularly at periods > 100 s. This region was affected by the Keweenaw Mid-continent Rift (~ 1.1 Ga), and structural perturbations or compositional anomalies relating to the effects of the rifting event may explain the lowered phase velocities. Anisotropic anomalies in this region are poorly constrained by our present data set; inclusion of data from stations south of the Canada–USA border will be required to provide crossing interstation paths over Lake Superior.

The \sim ENE–WSW direction of anisotropy in the western Superior region appears to be pervasive throughout most of the period range covered by the surface wave studies. Inspection of Rayleigh wave depth sensitivity kernels (Fig. 13) suggests that this period range corresponds approximately to a depth range that spans the lowermost crust, lithospheric mantle and asthenospheric mantle (assuming an average lithospheric thickness of ~ 150 – 220 km *cf.* Darbyshire *et al.* 2007). Tectonic maps of the western Superior region show an amalgamation of subprovincial belts whose boundaries trend in an E–W to ENE–WSW direction. The anisotropy

resolved at the shorter and intermediate periods likely corresponds to large-scale crustal and lithospheric structures associated with the assembly of the western Superior Province by progressive accretion of magmatic arc complexes (e.g. Thurston *et al.* 1991; Calvert *et al.* 1995; Percival 1996). The longest surface wave periods (160 s) are most sensitive to velocity structure in the lowermost lithosphere and sublithospheric mantle. Fast directions of anisotropy align with the direction of absolute plate motion, suggesting that the azimuthal anisotropy results largely from asthenospheric flow beneath the craton. The small amplitudes of phase-velocity anisotropy at 90–110 s period may suggest a decrease in anisotropy at depths corresponding to the mid-lower lithosphere.

In the eastern part of the study region, the anisotropy fast direction at the longest periods is close (within $\sim 10^\circ$ – 20°) to the direction of absolute plate motion, suggesting again that present-day asthenospheric flow contributes significantly to the seismic anisotropy at depth. At shorter periods, where the dominant fast direction is approximately NW–SE, the cause of the anisotropy cannot be as easily related to tectonic structure as it is in the west. The boundaries of the subprovinces of the Superior Craton do not have a trend approximately E–W, and the region's major tectonic boundary, the Grenville Front, lies in a roughly NE–SW orientation. However, three distinct tectonic features within the eastern region do exhibit a NW–SE orientation, and may contribute to the seismic anisotropy within the lithospheric mantle:

(1) The 2.5–2.45 Ga Matachewan dyke swarm (Ernst & Buchan 2001) radiates from a presumed hotspot centre located in south-eastern Ontario—the centre of the swarm is located in the vicinity of stations KLBO and BUKO (Fig. 1). Through northeastern Ontario, the dykes run in an N–S to NW–SE alignment. The area covered by the dyke swarm extends across most of eastern Ontario, with a spatial extent of ~ 500 km. Structural preferred orientation of lithospheric fabric due to the formation of the dyke swarms may contribute to seismic anisotropy in the upper lithospheric mantle (*cf.* correlation between anisotropy fast directions and kimberlite dyke trends in the Slave Province, e.g. Snyder & Bruneton 2007).

(2) The West Quebec Seismic Zone is characterized by NW–SE-trending bands of active seismicity and extends into eastern Ontario as far as Lake Timiskaming (vicinity of stations KILO and HSMO; Fig. 1) and Kapuskasing (vicinity of station KAPO; Fig. 1). The seismicity is believed to be associated with a system of faults formed in the Palaeozoic as a result of rifting across the region (Adams & Basham 1991). The resulting structural trends are thought to play a role in the distribution of *SKS* fast directions in the easternmost part of the study region (Frederiksen *et al.* 2006).

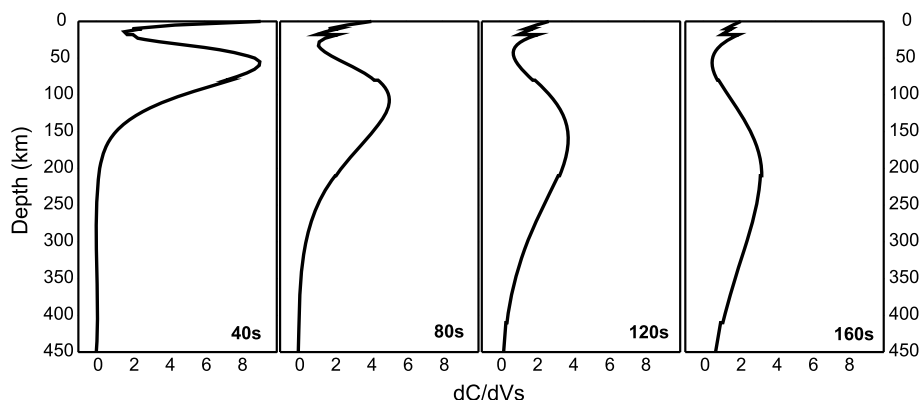


Figure 13. Rayleigh wave sensitivity kernels for periods between 40 and 160 s, illustrating the depth range sampled by the surface waves in this study.

(3) Eastern Ontario and western Quebec have been affected by the passage of eastern North America over the Great Meteor hotspot, whose track can be inferred from surface features related to volcanic activity (e.g. Heaman & Kjarvgaard 2000). Clusters of kimberlites, progressively younging to the SE, have been located in the vicinity of stations VIMO, KILO and HSMO (Fig. 1), and the Monteregian hills in southwest Quebec (east of station ALFO; Fig. 1) are also associated with the hotspot track (e.g. Crough 1981). The presumed hotspot track has an NW–SE alignment. Changes in physical or compositional properties between the hotspot-affected mantle along this track and the surrounding mantle may contribute in some way to anisotropy in the region, though the mechanism and effects are not clear.

In addition, while many zones of continental convergence exhibit anisotropy fast directions parallel to the orogenic belts, orogen-perpendicular fast directions, interpreted to correspond to lower lithosphere fabric, have been inferred in certain regions such as the Appalachian thrust belt in the northeastern USA (Levin *et al.* 2000). The orientation of the fabric was interpreted to arise from lithospheric thinning following the episode of orogeny. Whether this scenario might be applied to the Grenville orogeny is uncertain, but it remains a potential factor in explaining the lithospheric fast directions in the east.

Deschamps *et al.* (2008b) explained a pervasive NNW–SSE fast direction of anisotropy in the lower lithosphere of the eastcentral USA as attributable to past North American plate motion in the time period following the orogenic events that affected their study region, during which the lithosphere was gradually thickening and thus preserving the palaeo plate motion. Such a hypothesis is perhaps of relevance to the eastern part of our study region, given the role of the Grenville orogeny in the evolution of the lithosphere. However, this must remain a matter for speculation, since absolute plate motions in the Precambrian and Palaeozoic are not constrained.

The rotation from NW–SE to WNW–ESE fast directions with increasing surface wave period above 140 s likely reflects a gradual change in sampling from the lower lithosphere to the upper asthenosphere, given the apparent lithospheric thicknesses in the region (Darbyshire *et al.* 2007). We can speculate that this trend continues to periods greater than those resolved in this study, leading to a close correspondence between surface wave fast directions and absolute plate motion in both the east and west for periods where sampling is dominated by an asthenospheric signal, invoking present-day asthenospheric flow as the dominant mechanism for azimuthal anisotropy at depths greater than ~200–250 km.

It is clear from this study that, while both SKS splitting measurements and the surface wave tomography appear to give robust results in the east, the relationship between them is far more complex than that inferred in the west. Multiple anisotropic layers undoubtedly play a role, but their tectonic interpretation remains uncertain. We anticipate that future studies using seismic data from the eastern Ontario stations together with new networks across western Quebec may provide valuable information in piecing together the tectonic puzzle.

The resolution of asthenospheric azimuthal anisotropy by surface wave studies has led to a number of different inferences for the patterns and strength of present-day subcontinental flow. Compelling evidence for continental-scale asthenospheric flow comes from Australia (e.g. Debayle & Kennett 2000; Simons *et al.* 2002; Debayle *et al.* 2005), where a re-organization of azimuthal anisotropy takes place at ~150 km depth, into a coherent N–S-trending pattern that persists to ~250 km depth. The fast direction of anisotropy in this

depth range is approximately parallel to absolute plate motion, and has been interpreted to arise from deformation at the base of the continental portion of the Australian plate arising from the rapid passage of the plate over the underlying mantle. In contrast, while Pedersen *et al.*'s (2006) model shows significant coherent azimuthal anisotropy in the 200–250 km depth range beneath Fennoscandia, the fast direction is not parallel to plate motion, leading to an interpretation of a more complex convective flow, not primarily due to the lithospheric plate motion.

While Debayle *et al.* (2005) argue on the basis of their global surface wave model that Australia is the only continent to exhibit azimuthal anisotropy consistent with absolute plate motion in the 150–300 km depth range, evidence from continental-scale (Marone & Romanowicz 2007) and regional-scale (Deschamps *et al.* 2008a,b) surface wave studies suggests that much of North America shows patterns of anisotropy consistent with sublithospheric mantle flow parallel to absolute plate motion. Marone & Romanowicz (2007) use a joint inversion of multimode surface wave and SKS splitting data to argue that many other large-scale surface wave studies underestimate continental sublithospheric azimuthal anisotropy due to a reduction in surface wave sensitivity below ~250 km depth, and that horizontal shear due to the motion of a tectonic plate over the underlying mantle may in fact be more pervasive than suggested by Debayle *et al.* (2005). The study of eastcentral North America by Deschamps *et al.* (2008a,b) suggests three distinct layers of azimuthal anisotropy. Rayleigh waves at long periods exhibit phase-velocity anisotropy with a uniform fast-propagation direction parallel to current absolute plate motion and parallel to fast-propagation directions inferred from SKS splitting. The depth range associated with the longest sampled periods is estimated as 150–250 km, based on the inversions for anisotropic V_s profiles (Deschamps *et al.* 2008b), and the anisotropy is interpreted as arising from present-day deformation associated with asthenospheric flow.

9 CONCLUSIONS

We have used a tomographic inversion procedure to calculate anisotropic phase-velocity maps from sets of two-station Rayleigh wave dispersion curves. The path coverage allows the resolution of isotropic phase velocity within the northern Ontario Superior Province on a scale of ~200 km. Dense azimuthal coverage of interstation paths allows the resolution of at least two distinct regions of anisotropy across the region, representing a lateral resolution scale of ~500 km.

Tests on damping and smoothing parameters, model resolution and trade-offs between isotropic and anisotropic structures indicate that careful analysis of regularization and degree of model heterogeneity is of great importance in regional anisotropic surface wave tomography, in which the station spacing and path coverage may not be optimal. In particular, regions of high isotropic phase-velocity heterogeneity over length scales shorter than the lateral resolution of the model may lead to significant leakage between isotropic and anisotropic structures.

The average phase velocities across northern and eastern Ontario are up to 3 per cent higher than those derived from the global reference model AK135, and correspond closely to the 'CANSND' average Canadian Shield dispersion curve derived by Brune & Dorman (1963) from multiple two-station Rayleigh wave measurements. Above ~140 s period, the average phase velocity is close to that of AK135. Isotropic phase-velocity anomalies of up to ± 2 per cent around the regional average are resolved for the study region.

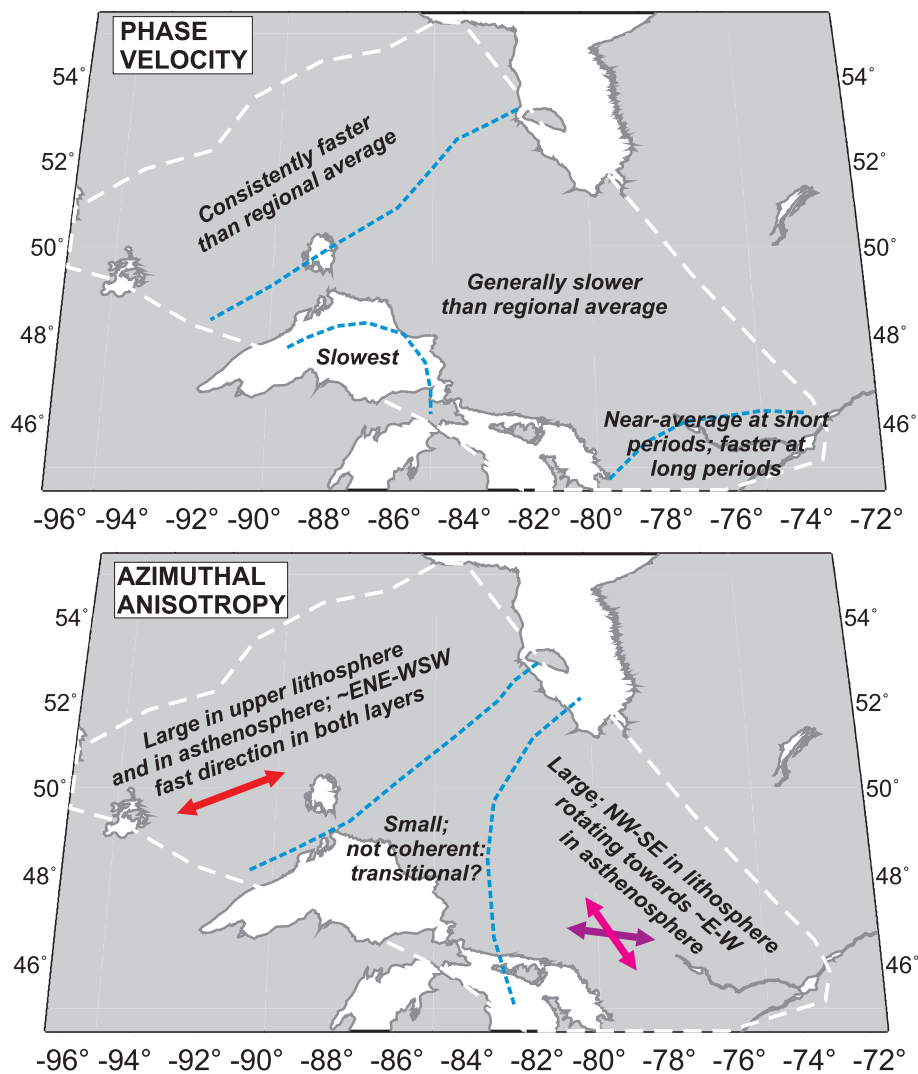


Figure 14. Summary of the main divisions in isotropic phase velocities and azimuthal anisotropy for the study region. Blue dashed lines mark the approximate boundaries where properties change; white dashed lines mark the region resolved by the surface wave study.

Fig. 14 summarizes the significant features of the anisotropic phase-velocity maps. The western Superior region is characterized by higher than average isotropic phase velocities and a pervasive ENE–WSW-trending fast direction of anisotropy throughout the period range of the data set. At shorter periods, the anisotropy likely results from structural fabric related to the assembly of the Superior Province, whereas the longest-period data likely indicate the direction of sublithospheric flow related to present-day plate motion. The correspondence between fast directions for ‘frozen’ lithospheric and current asthenospheric anisotropy can explain the large amplitude of the *SKS* splits measured in this region.

The central region has relatively weak anisotropy and the fast direction does not appear to follow a coherent pattern, suggesting a zone of transition between the distinct anisotropies of the east and west. Isotropic phase velocities are generally slower than average, with the lowest velocities beneath Lake Superior. We speculate that the relatively low velocities may arise from anomalous lithospheric structure due to the influence of the Mid-continent Rift on the southernmost part of the craton.

In the east, isotropic phase velocities are mostly slower than the regional average, with the exception of the far SE at periods

>80 s. The dominant fast direction of anisotropy is NW–SE for all but the longest periods. This alignment may result from lithospheric structural trends related to Proterozoic dyke swarms, Palaeozoic rifting or the passage of the Great Meteor hotspot. At the longest periods, the fast direction is broadly consistent with absolute plate motion and thus is likely dominated by present-day sublithospheric flow.

The use of the tomographic inversion technique as applied to multiple two-station phase-velocity measurements provides new information about the internal structure of the Superior Craton and its neighbouring mobile belts on a subprovincial scale, and allows us to resolve multiple layers of lithospheric and asthenospheric anisotropies.

ACKNOWLEDGMENTS

The operation of the POLARIS seismograph network would not be possible without the dedication of the researchers, technicians and students who have contributed to the deployment and maintenance of the array. Thanks are due in particular to Isa Asudeh, POLARIS Operations Manager at the Geological Survey of Canada.

The installation and operation of the broad-band seismograph network in southern Ontario and surrounding regions was funded by the Canada Foundation for Innovation, the Ontario Innovation Trust Fund, the Natural Sciences and Engineering Research Council of Canada and Ontario Power Generation. Funding for northern Ontario seismograph stations was provided by the FedNor.

Surface wave seismograms were extracted from POLARIS/FedNor and CNSN data archived by the Canadian National Data Centre, Ottawa.

We thank Vadim Levin, Jeffrey Park and Gabi Laske for their insightful and helpful manuscript reviews.

The figures in this manuscript were produced using the GMT software of Wessel & Smith (1991).

GEOTOP Publication number 2008-0028.

REFERENCES

- Adams, J. & Basham, P., 1991. The seismicity and seismotectonics of eastern Canada, in *Neotectonics of North America, Decade Map*, Vol. 1, pp. 261–276, eds Slemmons, D.B., Engdahl, E.R., Zoback, M.D. & Blackwell, D.D., Geological Society of America, Boulder, Colorado.
- Argus, D.F. & Gordon, R.G., 1991. No-net-rotation model of current plate velocities incorporating plate motion model NUVEL-1, *Geophys. Res. Lett.*, **18**, 2039–2042.
- Beucler, É. & Montagner, J.-P., 2006. Computation of large anisotropic seismic heterogeneities (CLASH), *Geophys. J. Int.*, **165**, 447–468.
- Brune, J. & Dorman, J., 1963. Seismic waves and Earth structure in the Canadian Shield, *Bull. seism. Soc. Am.*, **53**, 167–210.
- Bruneton, M., Farra, V., Pedersen, H.A. & the SVEKALAPKO Seismic Tomography Working Group, 2002. Non-linear surface wave phase velocity inversion based on ray theory, *Geophys. J. Int.*, **151**, 583–596.
- Calvert, A.J., Sawyer, E.W., Davis, W.J. & Ludden, J.N., 1995. Archaean subduction inferred from seismic images of a mantle suture in the Superior Province, *Nature*, **375**, 670–674.
- Chevrot S. & Zhao, L., 2007. Multiscale finite-frequency Rayleigh-wave tomography of the Kaapvaal craton, *Geophys. J. Int.*, **169**, 201–215, doi:10.1111/j.1365-246X.2006.03289.x.
- Crough, W.T., 1981. Mesozoic hotspot epeirogeny in eastern North America, *Geology*, **9**, 2–6.
- Darbyshire, F.A. *et al.*, 2004. A first detailed look at the Greenland lithosphere and upper mantle, using Rayleigh wave tomography, *Geophys. J. Int.*, **158**, 267–286.
- Darbyshire, F.A., Eaton, D.W., Frederiksen, A.Ws. & Ertolahti, L., 2007. New insights into the lithosphere beneath the Superior Province from Rayleigh wave dispersion and receiver function analysis, *Geophys. J. Int.*, **169**, 1043–1068, doi:10.1111/j.1365-246X.2006.03259.x.
- Debayle, E. & Kennett, B.L.N., 2000. The Australian continental upper mantle: structure and deformation inferred from surface waves, *J. geophys. Res.*, **105**, 25 423–25 450.
- Debayle, E., Kennett, B. & Priestley, K., 2005. Global azimuthal seismic anisotropy and the unique plate-motion deformation of Australia, *Nature*, **433**, 509–512.
- Deschamps, F., Lebedev, S., Meier, T. & Trampert, J., 2008a. Azimuthal anisotropy of Rayleigh-wave phase velocities in the east-central US, *Geophys. J. Int.*, **173**, 827–843, doi:10.1111/j.1365-246X.2008.03751.x.
- Deschamps, F., Lebedev, S., Meier, T. & Trampert, J., 2008b. Stratified seismic anisotropy reveals past and present deformation beneath the east-central United States, *Earth planet. Sci. Lett.*, **274**, 489–498.
- Eaton, D., Frederiksen, A. & Miong, S.-K., 2004. Shear-wave splitting observations in the lower Great Lakes region; evidence for regional anisotropic domains and keel-modified asthenospheric flow, *Geophys. Res. Lett.*, **31**, doi:10.1029/2004GL019438.
- Eaton, D. *et al.*, 2005. Investigating Canada's lithosphere and earthquake hazards with portable arrays, *EOS, Trans. Am. geophys. Un.*, **86**(17), 169–176.
- Ernst, R.E. & Buchan, K.L., 2001. The use of mafic dyke swarms in identifying and locating mantle plumes, in *Mantle Plumes: Their Identification Through Time*, Vol. 352, pp. 247–265, eds Ernst, R.E. & Buchan, K.L., Geol. Soc. Am. Spec. Paper.
- Forsyth, D.W. & Li, A., 2005. Array analysis of two-dimensional variations in surface wave phase velocity and azimuthal anisotropy, in *Seismic Earth: Array Analysis of Broadband Seismograms, Geophysical Monograph Series*, Vol. 157, eds Nolet, G. & Levander, A., American Geophysical Union.
- Fouch, M. & Rondenay, S., 2006. Seismic anisotropy beneath stable continental interiors, *Phys. Earth planet. Inter.*, **158**, 292–320.
- Frederiksen, A.W., Ferguson, I.J., Eaton, D., Miong, S.-K. & Gowan, E., 2006. Mantle fabric at multiple scales across an Archean-Proterozoic boundary, Grenville Front, Canada, *Phys. Earth planet. Inter.*, **158**, 240–263.
- Frederiksen, A.W., Miong, S.-K., Darbyshire, F., Eaton, D., Rondenay, S. & Sol, S., 2007. Lithospheric variations across the Superior Province, Ontario, Canada: evidence from tomography and shear wave splitting, *J. geophys. Res.*, **112**, doi:10.1029/2006JB004861.
- Friederich, W., 2003. The S-velocity structure of the East Asian mantle from inversion of shear and surface waveforms, *Geophys. J. Int.*, **153**, 88–102.
- Heaman, L.M. & Kjarsgaard, B.A., 2000. Timing of eastern North American kimberlite magmatism: continental extension of the Great Meteor hotspot track? *Earth planet. Sci. Lett.*, **178**, 253–268.
- Hoffman, P.F., 1988. United Plates of America, the birth of a craton: early Proterozoic assembly and growth of Laurentia, *Ann. Rev. Earth planet Sci.*, **16**, 543–603.
- Kay, I., Sol, S., Kendall, J.-M., Thomson, C., White, D., Asudeh, I., Roberts, B. & Francis, D., 1999. Shear wave splitting observations in the Archean craton of western Superior, *Geophys. Res. Lett.*, **26**, 2669–2672.
- Kendall, J.-M., Sol, S., Thomson, C.J., White, D.E., Asudeh, I., Snell, C.S. & Sutherland, F.H., 2002. Seismic heterogeneity and anisotropy in the Superior Province, Canada: insights into the evolution of an Archean craton, in *The Early Earth: Physical, Chemical and Biological Development*, Vol. 199, pp. 27–44, eds Fowler, C.M.R., Ebinger, C.J. & Hawkesworth, C.J., Geol. Soc. London, Special Publication.
- Kennett, B.L.N., Engdahl, E.R. & Buland, R., 1995. Constraints on seismic velocities in the Earth from traveltimes, *Geophys. J. Int.*, **122**, 108–124.
- Lebedev, S. & van der Hilst, R.D., 2008. Global upper-mantle tomography with the automated multimode inversion of surface and S wave forms, *Geophys. J. Int.*, **173**, 505–518, doi:10.1111/j.1365-246X.2008.03721.x.
- Levin, V., Park, J., Brandon, M.T. & Menke, W., 2000. Thinning of the upper mantle during late Paleozoic Appalachian orogenesis, *Geology*, **28**, 239–242.
- Li, A., Forsyth, D.W. & Fischer, K.M., 2003. Shear wave velocity structure and azimuthal anisotropy beneath eastern North America, *J. geophys. Res.*, **108**(B8), 2262, doi:10.1029/2002JB002259.
- Ludden, J. & Hynes, A., 2000. The Lithoprobe Abitibi-Grenville transect: two billion years of crust formation and recycling in the Precambrian Shield of Canada, *Can. J. Earth Sci.*, **37**, 459–476.
- Marone, F. & Romanowicz, B., 2007. The depth distribution of azimuthal anisotropy in the continental upper mantle, *Nature*, **447**, 198–201, doi:10.1038/nature05742.
- Menke, W. & Abbott, D., 1990. *Geophysical Theory*, Columbia University Press, Irvington, NY.
- Montagner, J.-P. & Nataf, H.-C., 1986. A simple method for inverting the azimuthal anisotropy of surface waves, *J. geophys. Res.*, **91**, 511–520.
- Montagner, J.-P., Griot-Pommeroy, D.A. & Lavé, J., 2000. How to relate body wave and surface wave anisotropy? *J. geophys. Res.*, **105**, 19 015–19 027.
- Paige, C.C. & Saunders, M.A., 1982. LSQR: an algorithm for sparse linear equations and sparse least squares, *Assoc. Comput. Mach. Trans. Math. Software*, **8**, 43–71.
- Pedersen, H.A., Bruneton, M., Maupin, V. & SVEKALAPKO Seismic Tomography Working Group, 2006. Lithospheric and sublithospheric anisotropy beneath the Baltic Shield from surface-wave array analysis, *Earth planet. Sci. Lett.*, **244**, 590–605.
- Percival, J.A., 1996. Archean cratons, in *Searching for Diamonds in Canada, Geological Survey of Canada Open File*, Vol. 3228, pp. 11–15,

- eds LeCheminant, A.N., Richardson, D.G., DiLabio, R.N.W. & Richardson, K.A., Geological Survey of Canada, Ottawa.
- Prindle, K. & Tanimoto, T., 2006. Teleseismic surface wave study for S-wave velocity structure under an array: southern California, *Geophys. J. Int.*, **166**, 601–621.
- Rondenay, S., Bostock, M.G., Hearn, T., White, D.J., Wu, H., Senechal, G., Ji, S. & Mareschal, M., 2000a. Teleseismic studies of the lithosphere below the Abitibi-Grenville Lithoprobe transect, *Can. J. Earth Sci.*, **37**, 415–426.
- Rondenay, S., Bostock, M.G., Hearn, T., White, D.J. & Ellis, R.M., 2000b. Lithospheric assembly and modification of the SE Canadian Shield: Abitibi-Grenville Teleseismic Experiment, *J. geophys. Res.*, **105**, 13 735–13 754.
- Sebai, A., Stutzmann, E., Montagner, J.-P., Sicilia, D. & Beucler, E., 2006. Anisotropic structure of the African upper mantle from Rayleigh and Love wave tomography, *Phys. Earth planet. Inter.*, **155**, 48–62.
- Silver, P.G., 1996. Seismic anisotropy beneath the continents: probing the depths of geology, *Ann. Rev. Earth planet. Sci.*, **24**, 385–432.
- Silver, P.G. & Kaneshima, S., 1993. Constraints on mantle anisotropy beneath Precambrian North America from a transportable teleseismic experiment, *Geophys. Res. Lett.*, **20**, 1127–1130.
- Simons, F.J., van der Hilst, R.D., Montagner, J.-P. & Zielhuis, A., 2002. Multi-mode Rayleigh wave inversion for heterogeneity and azimuthal anisotropy of the Australian upper mantle, *Geophys. J. Int.*, **151**, 738–754.
- Smith, M.L. & Dahlen, F.A., 1973. The azimuthal dependence of Love and Rayleigh wave propagation in a slightly anisotropic medium, *J. geophys. Res.*, **78**, 3321–3333.
- Snyder, D. & Bruneton, M., 2007. Seismic anisotropy of the Slave craton, NW Canada, from joint interpretation of SKS and Rayleigh waves, *Geophys. J. Int.*, **169**, 170–188.
- Sol, S., 2003. Teleseismic waveform analysis and velocity structure beneath the Western Superior Province: glimpses into the deeper architecture of an Archean craton, *PhD thesis*, Queens University, Canada.
- Thurston, P.C., Williams, H.R., Sutcliffe, R.H. & Stott, G.M. (eds), 1991. *Geology of Ontario*, Vol. 4, Ontario Geological Survey, Special Publication.
- Trampert J. & Woodhouse, J.H., 2003. Global anisotropic phase velocity maps for fundamental mode surface waves between 40 and 150 s, *Geophys. J. Int.*, **154**, 154–165.
- van der Lee, S. & Frederiksen, A., 2005. Surface wave tomography applied to the North American upper mantle, in *Seismic Data Analysis and Imaging with Global and Local Arrays*, *Geophysical Monograph*, Vol. 157, pp. 67–80, eds Nolet, G. & Levander, A., American Geophysical Union, Washington DC, USA.
- Wang, Z. & Dahlen, F.A., 1995. Spherical-spline parameterization of 3-dimensional earth models, *Geophys. Res. Lett.*, **22**, 3099–3102.
- Weeraratne, D.S., Forsyth, D.W., Fischer, K.M. & Nyblade, A.A., 2003. Evidence for an upper mantle plume beneath the Tanzanian Craton from Rayleigh wave tomography, *J. geophys. Res.*, **108**(B9), 2427, doi:10.1029/2002JB002273.
- Wessel, P. & Smith, W.H.F., 1991. Free software helps map and display data, *EOS, Trans. Am. geophys. Un.*, **72**, 441, 445–446.
- Zhang, X., Paulssen, H., Lebedev, S. & Meier, T., 2007. Surface wave tomography of the Gulf of California, *Geophys. Res. Lett.*, **34**, doi:10.1029/2007GL030631.